SEDIMENTOLOGY the journal of the International Association of Sedimentologists IAS

Sedimentology (2025) **72**, 2173–2200 doi: 10.1111/sed.70039

Sedimentology and geomorphology of tufa barrages on rock coast shore platforms

THOMAS W. GARNER* , J. ANDREW G. COOPER*† and ALAN SMITH†
**School of Geography and Environmental Science, Ulster University, Coleraine BT52 1SA, UK (E-mail: garner-t@ulster.ac.uk)*
†Discipline of Geology, School of Agriculture, Earth and Environmental Sciences, University of KwaZulu-Natal, P. Bag X54001, Durban 4000, South Africa

Associate Editor: Concha Arenas

ABSTRACT

Despite tufa deposits being widely distributed and increasingly recognised globally on rock coasts, their distribution in the tidal frame and geomorphology is poorly understood. The distribution, sedimentology and geomorphology of tufa barrages on supratidal rock coasts are assessed and their controls established. Tufa barrages are comprised of multiple facies including previously recognised tufa stromatolite, infaunal metazoan-bioturbated tufa, bryophyte phytoherm tufa and *Ulva* tufa, the latter of which has not previously been reported. These facies form an association, firmly placed in the supratidal zone, limited landward by the highest elevation of the shore platform (ca 9.5 m a.s.l.) and seaward by the high tide level (1.625 m a.s.l.). A clear ecological zonation of facies is defined by formative primary mediators (i.e. microbial communities, bryophytes and *Ulva intestinalis*) each of which influences barrage morphology. Lacking emergent and riparian vegetation, these biological controls differ from tufa in terrestrial settings. Barrages increase in size with decreasing elevation AMSL at a 0.01 significance level (n = 216); associated with the ecological zonation. Significant physical controls on barrage morphology include bedrock slope and topography (e.g. channelisation and bedrock steps). Tufa cascades occur across the shore platform in areas of high bedrock slope (ca 20 to 90°), while barrages occupy shallower slopes (ca 0 to 20°), and lacustrine and fluvial crusts develop across the full range of slopes. Barrage size decreases with bedrock slope. Greater understanding of the controls on tufa facies distribution and associated geomorphology enhances their utility as palaeoenvironment and sea-level indicators and archives.

Keywords rock coast, shore platform, tufa barrage, tufa stromatolite.

INTRODUCTION

Tufa, including tufa microbialite facies, is widely distributed on rocky coastlines, and deposited where carbonate-rich groundwater springs emerge in the supratidal zone (Forbes *et al.*, 2010; Smith *et al.*, 2011, 2018; Perissinotto *et al.*, 2014; Rishworth *et al.*, 2020; Cooper *et al.*, 2022). Their ecology (e.g. Rishworth *et al.*, 2017a, 2020), geochemistry (e.g. Dodd *et al.*, 2018), sedimentology and geomorphology (Edwards *et al.*, 2017; Smith *et al.*, 2018; Cooper *et al.*, 2022; Garner *et al.*, 2024) have been investigated. While terrestrial tufa deposits are established Quaternary palaeoclimate and palaeoenvironment archives (Pedley, 1987; Andrews, 2006; Capezzuoli *et al.*, 2014), supratidal tufa deposits have the added potential to act as palaeo-sea-level indicators (Rishworth *et al.*, 2020; Garner *et al.*, 2025). An understanding of their geomorphology and underlying

© 2025 The Author(s). *Sedimentology* published by John Wiley & Sons Ltd on behalf of International Association of Sedimentologists.
This is an open access article under the terms of the Creative Commons Attribution License, which permits use, distribution and reproduction in any medium, provided the original work is properly cited.

controls is required if their utility is to be fully realised.

This paper focuses specifically on tufa barrage macro-structures or macro-morphology on rock coasts and aims to (i) document their form and distribution and (ii) investigate the underlying geomorphological controls. This is achieved through the:

1 qualitative measurement of distribution of tufa occurrences;
2 description and analysis of individual tufa systems through UAV-photogrammetry-derived orthomosaic and DSM visualisation;
3 summary of groundwater spring and barrage pool physico-chemistry;
4 sedimentological analysis of barrage-forming facies;
5 measurement and correlation analysis of tufa barrage morphometric and physical parameters (elevation and slope); and
6 testing of physical controls on barrage tufa geomorphology through orthomosaic and DSM subsite visualisation.

Tufa distribution, geomorphology and controls

Tufa deposits have a global distribution (Ford & Pedley, 1996; Pentecost, 2005) and are primarily terrestrial deposits. Tufa deposits with marine influences, however, have been described (Flinn & Pentecost, 1995; Howie & Ealey, 2009, 2010; Faulkner & Crae, 2018; Rodríguez Guitián *et al.*, 2020), including the 'rock coast' tufa microbialite and shore platform stromatolite facies. These deposits have been documented in southern Africa (Smith *et al.*, 2011, 2018; Edwards *et al.*, 2017), Western Australia (Forbes *et al.*, 2010) and the north-east Atlantic (Smith *et al.*, 2018). Generalised facies distributions have been assessed (Cooper *et al.*, 2022) and structural and morphological nomenclatures proposed (Garner *et al.*, 2024). They are usually described as occurring in the supratidal to the high intertidal zone (Smith *et al.*, 2011, 2018; Perissinotto *et al.*, 2014; Edwards *et al.*, 2017; Rishworth *et al.*, 2017b, 2020; Dodd *et al.*, 2018, 2021; Cooper *et al.*, 2022; Forbes *et al.*, 2024).

A variety of distinct macrostructures or morphologies, including cascades, fluvial and lacustrine crusts, and barrages, have been recognised (Garner *et al.*, 2024). These include features of both spring deposits and fluvial tufa, based on a variable degree of channel confinement and the degree of input from groundwater springs, rainwater and runoff (Jones & Renaut, 2010); their similarities in morphology and genesis suggest many of the same controls on geomorphology as their terrestrial counterparts (Edwards *et al.*, 2017; Garner *et al.*, 2024). Barrages are a dominant component of the rock coast assemblage and are the focus of this paper.

In terrestrial systems, the morphology and formation of barrages are influenced by a range of complex abiotic and biotic factors and interactions. Biological controls include biomineralisation of organic tissue and surficial precipitation, as extracellular polymeric substances create a favourable environment for the precipitation of calcium carbonate (Riding, 1991; Arp *et al.*, 2001; Pentecost, 2005; Hägele *et al.*, 2006). Carbonate-precipitating microorganisms influence the growth and development of tufa and their micro-scale morphology (Merz-Preiß & Riding, 1999; Viles & Pentecost, 1999; Fuller *et al.*, 2011); and where micro-environments are amenable to growth, such as barrage crests (Fuller *et al.*, 2011), they can influence large-scale geomorphology.

Macrophytes and riparian vegetation commonly influence tufa initiation, formation and geomorphology. On barrage surfaces, macrophytes can act as favourable sites for calcium carbonate nucleation, as well as filtering sediment/organic matter and influencing hydrodynamics (Viles & Pentecost, 1999; Fuller *et al.*, 2011; Zhang *et al.*, 2023). Accumulated riparian vegetation debris within channels, including large woody debris (LWD), also greatly influences the initiation and development of tufa barrages (Pedley, 1980; Viles & Pentecost, 1999; Pentecost *et al.*, 2001; Carthew *et al.*, 2003; Fuller *et al.*, 2011; Florsheim *et al.*, 2013; Profe *et al.*, 2016), and, once established, barrages can trap and retain floating debris, provide sites for precipitation (Zhang *et al.*, 2023) and retention of nutrients (Carter & Marks, 2007; Compson *et al.*, 2009).

The hydrodynamic conditions of waters supersaturated with respect to $CaCO_3$ are a primary influence on tufa formation, distribution and geomorphology. In the correct conditions, a decrease in fluid pressure and/or increase in the rate of CO_2 degassing results in calcium carbonate precipitation (Herman & Lorah, 1988; Lu *et al.*, 2000; Chen *et al.*, 2004; Pentecost, 2005; Hammer *et al.*, 2007; Hammer, 2009; Zhang *et al.*, 2023) and once initiated, this can lead to a positive feedback further favouring

© 2025 The Author(s). *Sedimentology* published by John Wiley & Sons Ltd on behalf of International Association of Sedimentologists,

precipitation, exceeding destructive mechanical erosion and chemical dissolution (Chen *et al.*, 2004; Chan & Goldenfeld, 2007; Hammer *et al.*, 2007, 2008; Chin *et al.*, 2014; Zhang *et al.*, 2023).

The physical environment and substrate topography are intrinsically coupled with the hydrodynamics of tufa-bearing systems. Rapid tufa precipitation in high-energy hydraulic regimes occurs through lowering of water pressure and rapid CO_2 degassing (Lorah & Herman, 1988; Drysdale & Gillieson, 1997; Hammer *et al.*, 2007). As a result, the slope on which tufa barrages form is a major control, with steeper slopes promoting tufa accretion and decreasing barrage pool size (Pentecost, 2005; Hammer *et al.*, 2007; Wolfgang & Gabrovsek, 2009; Florsheim *et al.*, 2013). The subsequent alteration of slope due to barrage development further modifies flow dynamics, promoting precipitation in a positive feedback (Chan & Goldenfeld, 2007; Hammer *et al.*, 2007; Florsheim *et al.*, 2013).

Substrate topography also influences tufa geomorphology; channel width and/or the degree of channelisation can change the flow rate, channel-bed surface and size of air–water interface, which in turn influences the occurrence, distribution and geomorphology of barrages (Chen *et al.*, 2004; Fuller *et al.*, 2011; Florsheim *et al.*, 2013; Profe *et al.*, 2016). Breaks in slope such as bedrock steps and emergent boulders also create the potential for rapid flow acceleration and increased turbulence, resulting in lower water pressure and increased degassing, promoting precipitation and barrage formation (Hammer *et al.*, 2007; Fuller *et al.*, 2011; Florsheim *et al.*, 2013; Profe *et al.*, 2016).

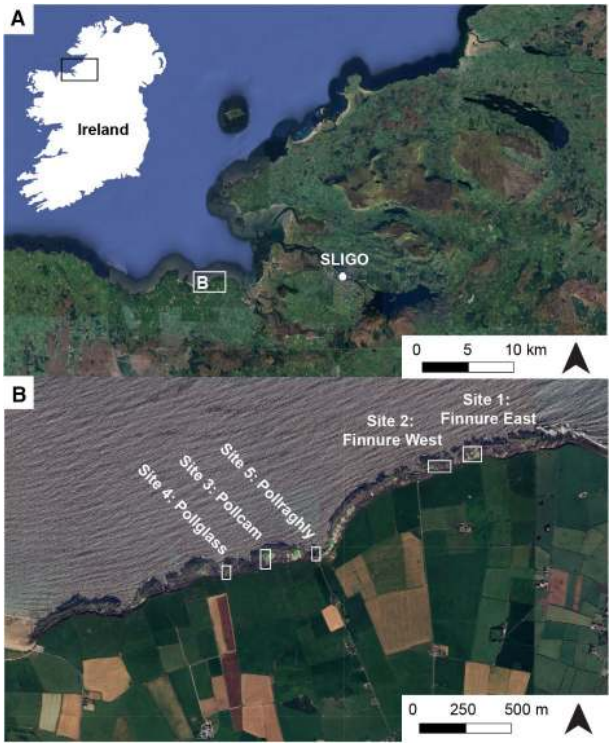


Fig. 1. Location of study area and sites. (A) Location of study area in Ireland (inset) and location of study area in relation to Sligo. (B) Location of study sites on the Pollraghly shore platform (Google Earth Pro, 2025).

STUDY AREA

A large supratidal shore platform in County Sligo, in western Ireland (Fig. 1A) is the site of multiple groundwater spring discharges and an array of tufa barrage features, presenting an ideal field site for investigation of the controls on morphology.

The study area geology comprises calcarenite limestone (Carboniferous Ballyshannon Limestone Formation) overlain by glacial tills derived from limestone and metamorphic lithologies (GSI, 2019, 2021). This bedrock forms a large supratidal seaward-dipping shore platform, ('type A: ramp'; Sunamura, 1992) that extends sub-tidally (Marine Institute, 2017) and is incised by small embayments or geos, called polls. The study area is within the Beltra-Sligo groundwater body area, a karstified aquifer dominated by conduit flow through epikarstic Dinantian Pure Bedded Limestones (GSI, 2004). The groundwater aquifer comprises interconnected solution-enlarged fissures and conduits (faults, joints and bedding planes) recharged by diffuse flow through permeable overlying till, rock outcrop and swallow holes and discharging northwards to the coast through streams, rivers, lakes and springs (GSI, 2004). A summary of groundwater spring *in situ* measurements are presented in the results.

The area has a temperate maritime climate, with high rainfall (1241.6 mm/year) and a south-west prevailing wind averaging 12.5 knots, with 94 knots maximum gusts (Met Éireann, 2024). The tidal range is mesotidal at 3.25 m (Jackson *et al.*, 2022), and modal wave energy is high with seasonal storm and extreme wave events occurring (Cooper *et al.*, 2004;

© 2025 The Author(s). *Sedimentology* published by John Wiley & Sons Ltd on behalf of International Association of Sedimentologists, *Sedimentology*, **72**, 2173–2200

O'Brien *et al.*, 2018). For example, during Storm Ophelia in 2017, maximum wave height was 18.5 m, and significant wave height was 4.41 m (O'Brien *et al.*, 2018). Storm waves traverse the shore platform and deposit a boulder/megaclastic ridge landward.

Numerous carbonate-rich groundwater springs precipitate tufa deposits along the platform terrestrial margin and adjacent shore platform. Five springs were chosen to capture a range of shore platform slopes and surface morphologies (Fig. 1B).

METHODS

In situ water measurements and sampling

Groundwater spring and pool water physico-chemistry was measured in the field, with measurements of temperature, pH and electrical conductivity (EC) taken using a Hach portable pH/dissolved oxygen meter and a Hanna portable pH/EC/TDS/temperature meter. Summary data are provided from sites 1 to 3 and site 5.

Representative samples of barrage deposits were collected and cut in section. The description of facies follows Pedley (1990), Riding (1991) Ford & Pedley (1996), Della Porta (2015) and morphology/macrostructure follows Garner *et al.* (2024).

Photogrammetry and morphometric/physical parameters

Aerial photography was undertaken using a UAV [DJI Mini 2/FC7303: image sensor: 1/2.3" CMOS, effective pixels: 12 MP, focal length: 24 mm (35 mm equivalent)] ca 30 m above ground level (AGL) in June 2024. Five to 10 ground control points were measured using differential GPS at each site in the co-ordinate system TM75/Irish Grid (EGM96 Geoid). Orthomosaics and DSMs were created using PIX4D to produce DSMs with sub-centimetre average ground sampling distances (GSD) [0.64 cm (site 5) to 0.88 cm (site 4)]. RMS errors between ±0.09 cm (site 4) and ±0.14 cm (site 1) indicate high accuracy. Data visualisation, analysis and measurement of morphometric parameters was performed in QGIS (Fig. 2C, D).

Morphometric parameters are adapted from Pentecost (2005) (Fig. 2D). The absolute thickness of tufa deposits cannot be derived from the orthomosaic or DSM; hence, vertical parameters (e.g. barrage drop wall height) do not necessarily represent the total thickness. Similarly, refraction at the water–air interface (He *et al.*, 2021) and the presence of floating masses of *Ulva intestinalis* in a few (ca 10) barrage pools obscure the true pool depth, resulting in vertical parameters representing a minimum value. Headwater and tailwater pool lengths are associated with a single barrage, with the latter being equivalent to inter-dam distance (IDD) of Pentecost (2005), that is, the headwater pool of one barrage is the tailwater pool of the adjacent upstream barrage.

In addition to 216 measured barrages, paired physical parameters (elevation and slope) derived from the DSM were also measured using QGIS. Elevation is cited as above mean sea level (AMSL), determined as −0.05964 m (i.e. MSL below OD Malin) (RPS Group, 2020). High tide and MSL are shown at 1.625 m and 0 m, respectively, on elevation maps (Jackson *et al.*, 2022).

The ThreePointMethod QGIS Python Plugin (Brach, 2023) was applied to DSMs to measure the dip of bedrock and the physical parameter 'deposit dip': a measurement of dip covering the whole barrage (i.e. including barrage and tailwater barrage pool) (Fig. 2E). An alternative measurement of dip (inter-barrage dip or the slope between the barrage crest top and the crest top of the barrage at the tailwater pool) was also calculated (Fig. 2E). The correlation and statistical significance of the inter-relationships of morphometric and physical parameters were tested through a Spearman's 'rho' Correlation test (two-tailed).

RESULTS

Study sites: Tufa spring distribution, water physico-chemistry and geomorphology

Tufa deposits are ubiquitous within the study area. Groundwater springs drain from the spring emergence over the shore platform seaward as channelised and non-channelised flow. Measurements of platform width (from backing cliff/vegetation to MSL) reveal a total platform area of ca 254.5 km^2 of which ca 34.2 km^2 (13.4%) is covered with active and inactive tufa deposits.

Site 1: Finnure east

The shore platform at Finnure East is a wide (57 to 81 m; measured from backing cliff/vegetation to MSL) supratidal platform of complex topography with a general seaward dip of 6.4°. The

© 2025 The Author(s). *Sedimentology* published by John Wiley & Sons Ltd on behalf of International Association of Sedimentologists,

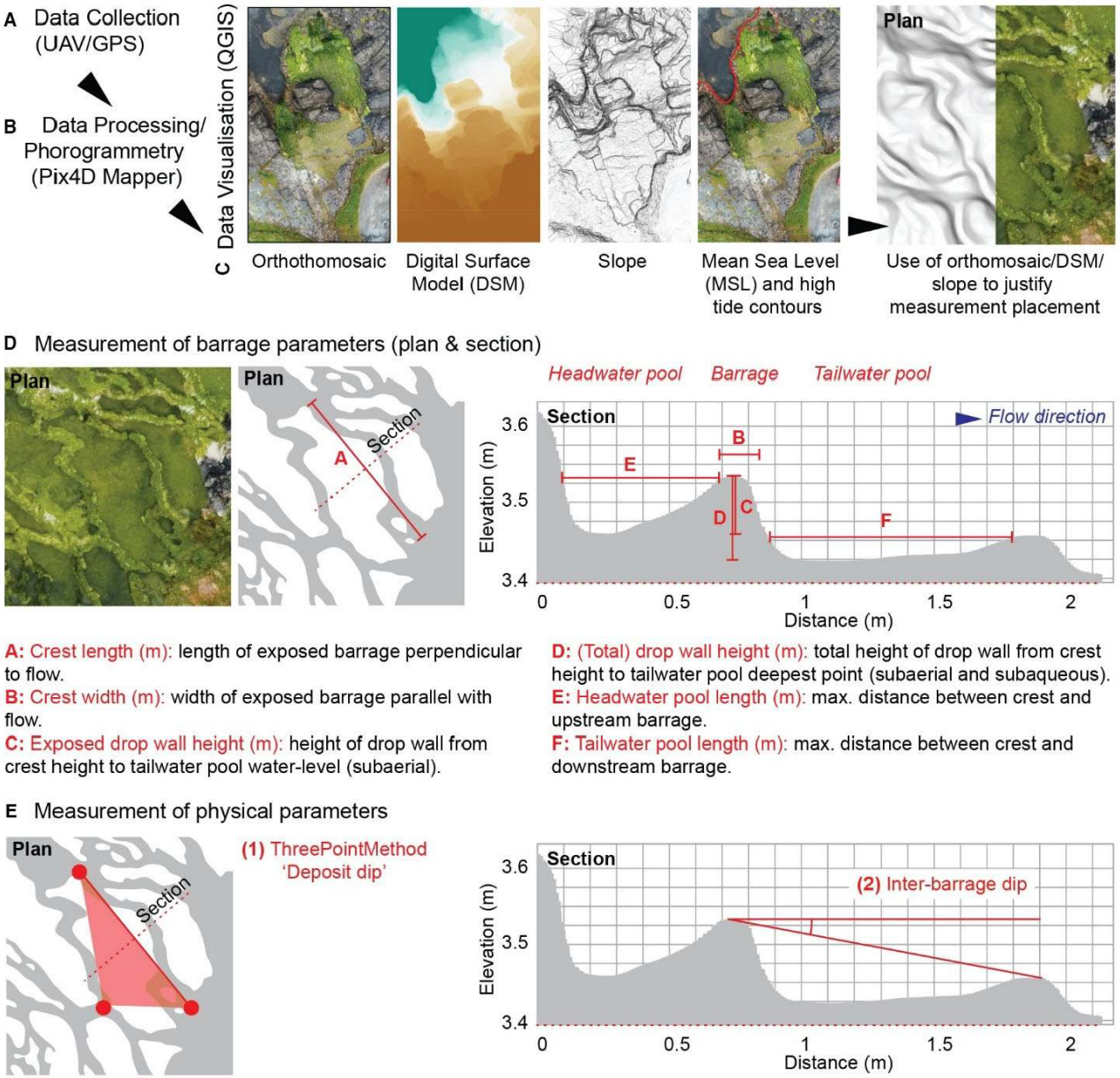


Fig. 2. Diagrammatic method for (A) data collection, (B–C) processing and visualisation, and (D) measurement of morphometric parameters (adapted from Pentecost, 2005) of barrages and (E) measurement of physical parameters.

platform is mostly exposed bedrock (Fig. 3A); with storm deposits of granule-boulder-sized clasts at the platform back and in topographic lows. Groundwater emerges from discrete springs (Fig. 3B), the largest and most productive of which flows onto the platform at 7.77 m a.s.l.; however, it likely emerges in the hinterland. Minor springs emerge from bedrock joints at 5.59 m, 5.72 m and 5.94 m a.s.l. and from under storm beach deposits at 6.95 m. Tufa deposition is wholly absent from areas of large flat bedrock in the extreme upper shore platform, which are colonised by filamentous algae, vascular plants and bryophytes. Water flows through topographical lows, bifurcating around positive topography forming a complex pattern of tributaries and distributaries. Tufa deposits vary in geomorphology and degree of flow confinement or channelisation, primarily forming large channelised barrages, unchannelised

© 2025 The Author(s). *Sedimentology* published by John Wiley & Sons Ltd on behalf of International Association of Sedimentologists, *Sedimentology*, **72**, 2173–2200

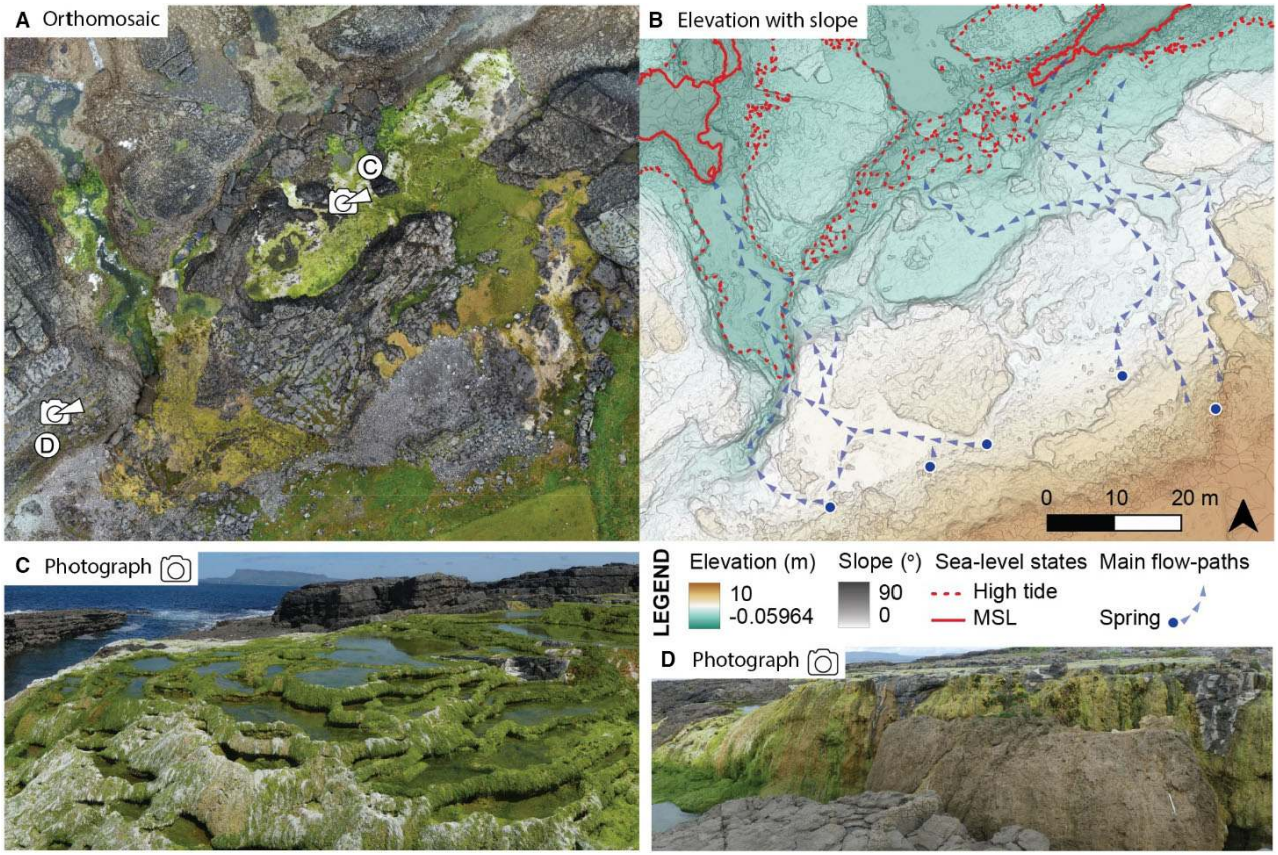


Fig. 3. Site 1: Finnure East. (A) Orthomosaic. (B) Elevation (m) with slope (degrees; 50% transparency), with high tide (1.56536 m above OD Malin), MSL (−0.05964 m above OD Malin), springs and main flow-paths. (C, D) Site photographs, for direction see panel A.

'delta'-like barrage features (Fig. 3C), cascades (Fig. 3D) and discharge aprons of lacustrine and fluvial crust. Large tufa deposits are deposited down to 1.93 ± 0.75 m a.s.l. (Fig. 3B).

Site 2: Finnure west

At Finnure West, a 34 to 72 m-wide supratidal platform of complex topography, with an overall 6° seaward dip. Minor accumulations of cobble-boulder clasts are present at the rear of otherwise bare bedrock (Fig. 4A). Groundwater springs emerge from a single karstified bedding plane between 3.79 m a.s.l. and 5.81 m a.s.l. depending on bedding plane elevation (Fig. 4B). Flow paths follow topographic lows in bedrock, bifurcating around topographic highs and forming a complex pattern of tributaries and distributaries (Fig. 4B, D). There is limited topographic confinement of flow, especially in the west; however, the occurrence of a large bedrock high seaward of springs results in a convoluted shore-parallel flow. Tufa deposition occurs as coalescing cascades at the spring line emergence and downstream barrages (Fig. 3C), with deposition ceasing at the base of a cascade at ca 1.6 m a.s.l.

Site 3: Pollcam

The Pollcam shore platform has a near-uniform slope of 4.9°, consistent with bedding over its 74 to 81 m width. Primarily exposed bedrock, the platform has scattered boulder-sized clasts and minor landward accumulations (Fig. 5A). A single discrete spring at 7.42 m a.s.l. emerges as a point feature on a karstified bedding plane (Fig. 5B) and flows over the shore platform as a large apron, unconfined by bedrock topography, with the only notable topography a single step in bedding (Fig. 5E). Tufa deposits occur as fluvial crusts and barrages

© 2025 The Author(s). *Sedimentology* published by John Wiley & Sons Ltd on behalf of International Association of Sedimentologists,

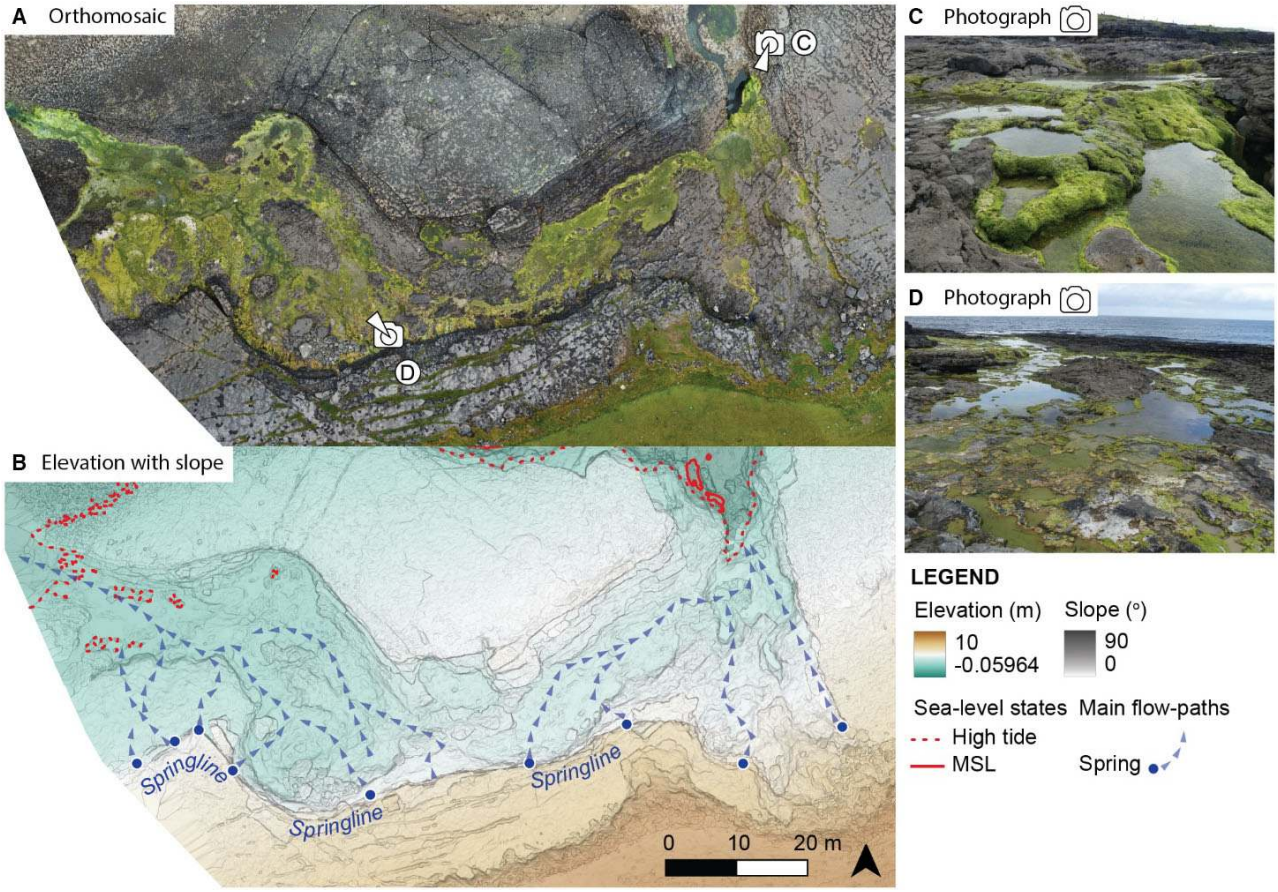


Fig. 4. Site 2: Finnure West. (A) Orthomosaic. (B) Elevation (m) with slope (degrees; 50% transparency), with high tide, MSL, springs and main flow-paths. (C, D) Site photographs, for direction see panel A.

(Fig. 5C, D) to the lowest elevation at 1.88 ± 0.7 m a.s.l.

Site 4: Pollglass

Pollglass has the narrowest shore platform (47 m wide, reduced to 30 m at a poll) and a consistent slope of 8.7° defined by bedding. It is backed by minor accumulations of cobble-boulder-sized clasts and a carbonate-cemented cliff of diamicton (Fig. 6A). At least two springs emerge at Pollglass; one emerges from a karstified joint at 7.05 m a.s.l., and the other is obscured by megaclast accumulations at least 6.91 m a.s.l. (Fig. 6B). Flow paths follow topographic lows and include strongly channelising flow in narrow channels (Fig. 6C) and unchannelised discharge aprons with negligible topographical constraint. Tufa deposits from the spring occur as fluvial and lacustrine crust on bedrock to around 2.17 m a.s.l.

Site 5: Pollraghly

The shore platform at Pollraghly is at a greater average elevation than the other sites, is of variable width (47 m at headlands and 27 m at a poll). The shore platform has a stepped topography, with the two gently dipping (3.8°) upper and lower shore platforms separated by small cliffs (Fig. 7A). Groundwater springs flow onto the shore platform at 10.58 m a.s.l. from a spring that emerges at ca 12 m a.s.l. (Fig. 7B). No tufa deposition occurs at the spring emergence or until ca 9.5 m a.s.l. where water flows over a bedrock step. Flow then bifurcates into two flow paths, with tufa deposited as barrages (Fig. 7C) and cascades (Fig. 7D) to ca 2.6 m a.s.l.

Groundwater spring and barrage pool in situ water measurements

Groundwater springs were uniform between Pollraghly shore platform sites, with comparable

© 2025 The Author(s). *Sedimentology* published by John Wiley & Sons Ltd on behalf of International Association of Sedimentologists, *Sedimentology*, **72**, 2173–2200

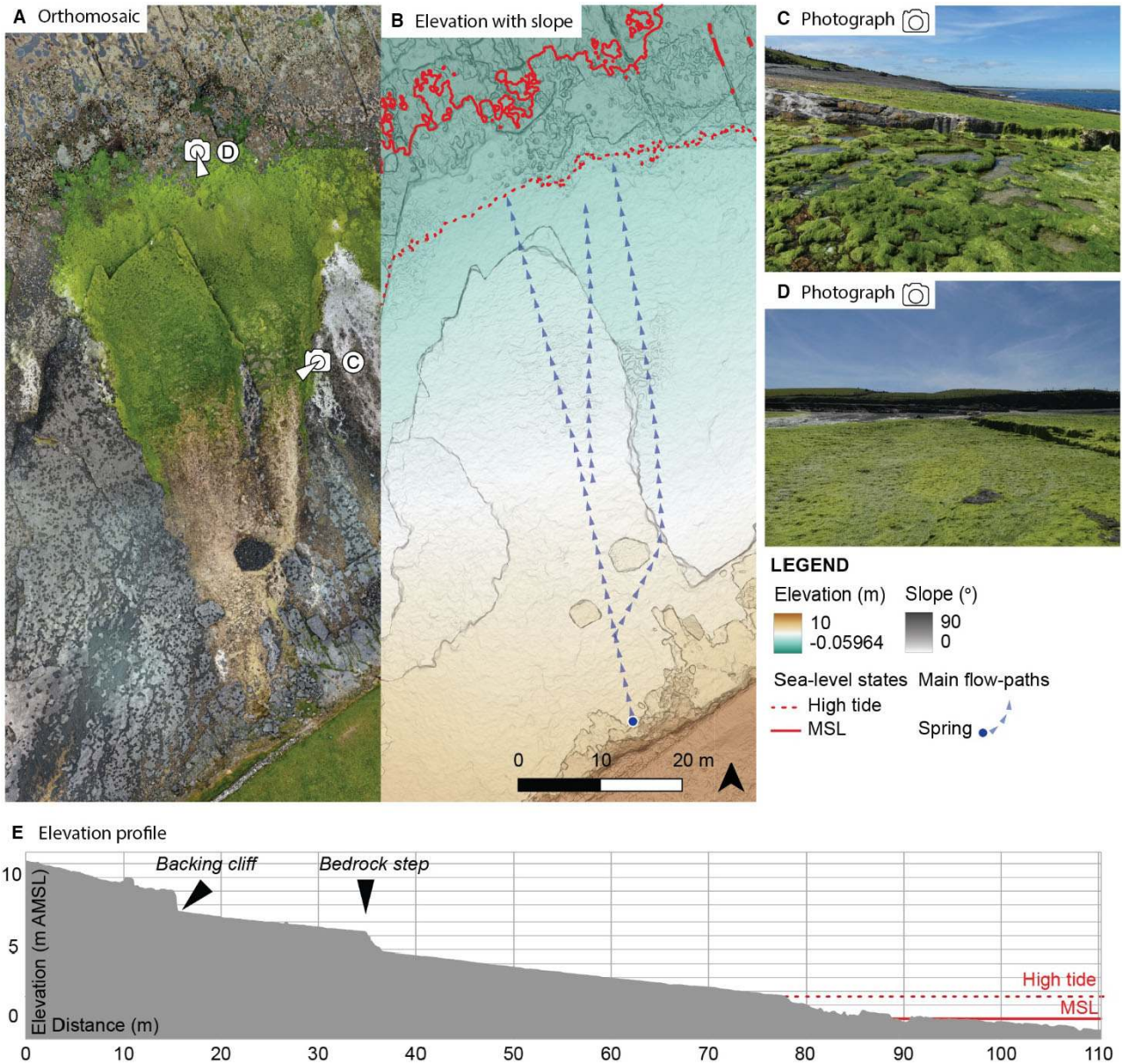


Fig. 5. Site 3: Pollcam. (A) Orthomosaic. (B) Elevation (m) with slope (degrees; 50% transparency), with high tide, MSL, springs and main flow-paths. (C, D) Site photographs, for direction see panel A. (E) Elevation profile.

temperature, pH and EC (Table 1). Tufa barrage pools are highly variable in their physico-chemistry, with temperature varying dependent on seasonal air temperature and pH exhibiting greater alkalinity during June (summer) and associated with barrage pools containing *U. intestinalis*. EC, considered a salinity proxy, is variable; in pools, it maintains an EC (0.7 to 0.87 mS/cm) comparable to groundwater springs in summer; however, at lower elevations, pools exhibit a substantial increase in EC, up to 73.2 mS/cm [site 3: Pollcam at 3.51 m a.s.l. in February (winter)] with vertical haloclines and poor mixing observed in November (autumn) and February (winter).

Tufa geomorphology

A variety of tufa macro-structures or macro-morphologies were recorded including cascades, barrages and fluvial and lacustrine crusts. Tufa

© 2025 The Author(s). *Sedimentology* published by John Wiley & Sons Ltd on behalf of International Association of Sedimentologists, *Sedimentology*, **72**, 2173–2200

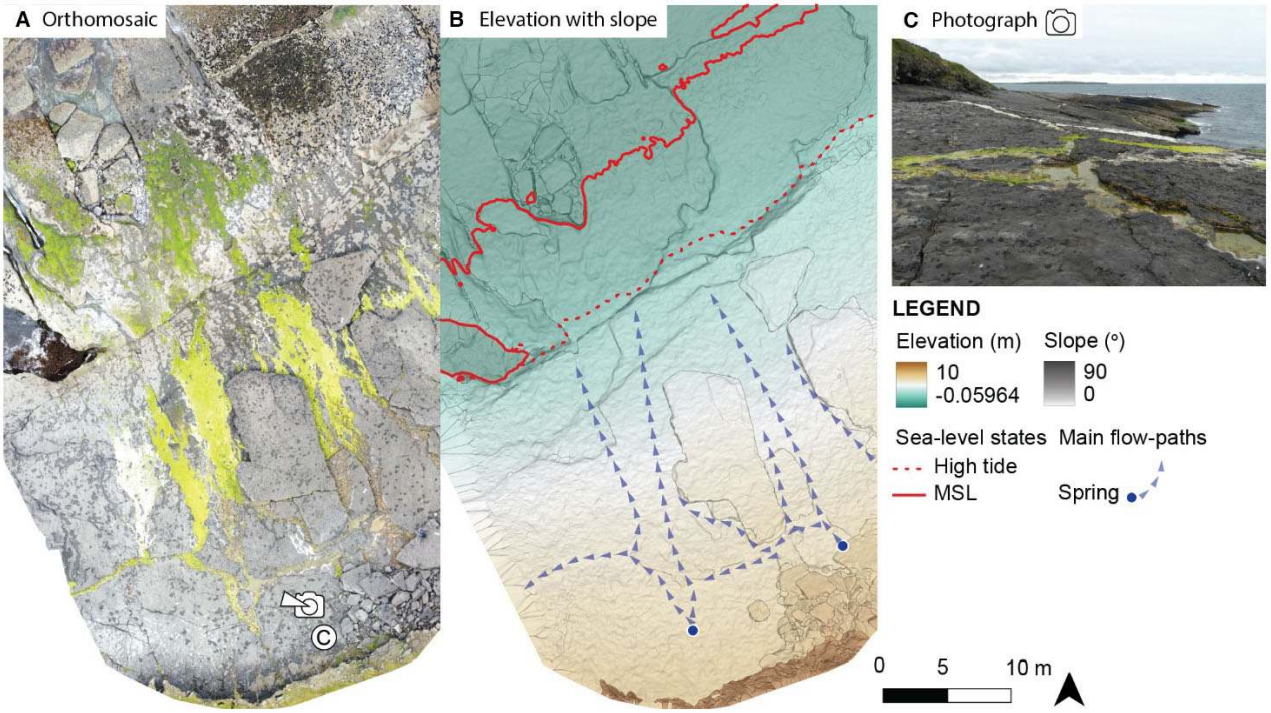


Fig. 6. Site 4: Pollglass. (A) Orthomosaic. (B) Elevation (m) with slope (degrees; 50% transparency), with high tide, MSL, springs and main flow-paths. (C) Site photograph, for direction see panel A.

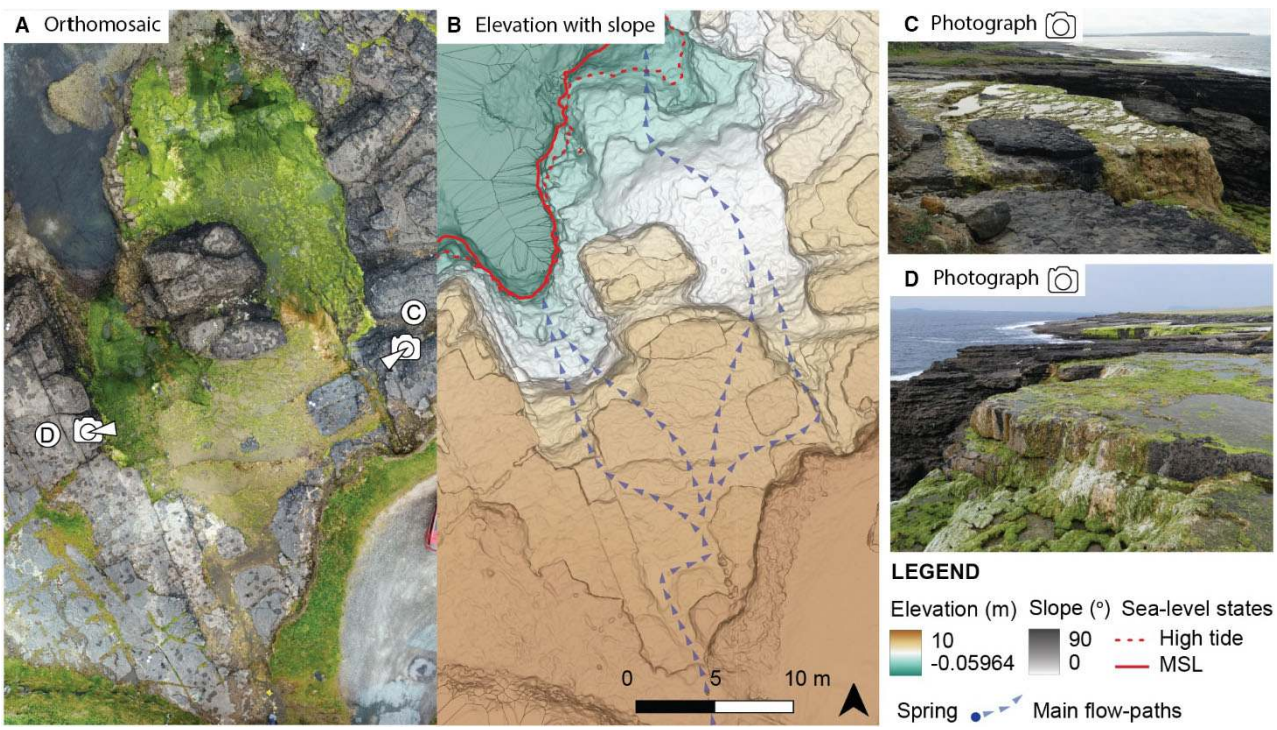


Fig. 7. Site 5: Pollraghly. (A) Orthomosaic. (B) Elevation (m) with slope (degrees; 50% transparency), with high tide, MSL, springs and main flow-paths. (C, D) Site photographs, for direction see panel A.

© 2025 The Author(s). *Sedimentology* published by John Wiley & Sons Ltd on behalf of International Association of Sedimentologists,

Table 1. Summary of groundwater spring and tufa barrage pool physico-chemistry data; temperature, pH and electrical conductivity (EC) collated from June (summer) 2024, November (autumn) 2025 and February (winter) 2025.

	Temperature (°C) Max–Min (Range)	pH Max–Min (Range)	EC (mS/cm) Max–Min (Range)
Groundwater springs	8.9–12.9 (4)	6.71–8.28 (1.57)	0.83–1.31 (0.48)
Tufa barrage pools	7.4–16.7 (9.3)	7.17–9.41 (2.24)	0.7–73.2 (72.5)

cascades (Figs 3D, 7D) form in a variety of settings, primarily where water flows over bedrock with a high angle of slope and can occur at any elevation along the shore platform profile. Barrages (Figs 3C, 4C, D, 5C and 7C) form where water flows over bedrock with a medium-low angle of slope; active barrages are characterised by the impoundment of water into barrage pools. Transitional cascades that may impound water, forming small barrages, are rare but present. Thin crusts (Fig. 6C) occur within rockpools where water flow is impounded by bedrock topography, forming small pools in bedrock depressions or basins, (lacustrine crusts) and in channelised or unchannelised or sheet flow (fluvial crusts).

Barrage facies and sedimentology

Barrages are common on the shore platform, and four distinct barrage-forming tufa facies were identified.

Facies 1: Bryophyte phytoherm tufa

Bryophyte phytoherm tufa comprises boundstone of acrocarpous mosses (e.g. *Eucladium verticllatum*), growing perpendicular to the precipitating surface in stacked parallel layers (ca 2 cm thick) and forming large (up to ca 30 cm diameter), frequently coalescing phytoherms (Fig. 8A, B). Leaves and stems are coated with micrite/sparry calcium carbonate coatings, forming a primary growth framework and porosity that varies according to the degree of bryophyte cementation (Fig. 8C). Bryophytes form the primary structure, although filamentous algae, cyanobacteria and biological inclusions (invertebrate remains including coleoptera elytra; vascular plants [e.g. *Armeria maritima, Plantago maritima* and *Cochlearia* cf. *officinalis*] phytoclasts) and minor lithic inclusions are also present.

Facies 2: Tufa stromatolite

Stromatolitic boundstone comprises a laminated micrite and sparite with coalescing columns, with lamination perpendicular to the precipitating surface, associated with radiating filamentous structures (Fig. 8F, G). Lamination is regular, comprising alternating couplets of dark thin (ca 150 to 250 μm) lamina of spar (crystals up to 250 × 250 μm in size) and light thick (ca 150 to 1300 μm) laminae of micrite (Fig. 8G). Radiating filamentous structures occur in small fans with inter-fan pores and low porosity (5.41%) with the facies containing a negligible clastic component (Fig. 9A). Externally, green-brown pustular and colloform microbial colonies are present; individual colloform heads directly relate to internal columnar structures (Fig. 8E). The facies has a low porosity, with minor pores present between columns and negligible inclusions.

Facies 3: Infaunal metazoan-bioturbated tufa

Infaunal metazoan-bioturbated tufa has extensive irregular and burrow porosity with micrite/sparite coatings (Fig. 8F, H). Irregular pores contain coated burrows with internal pores. Typically, burrows are unbranching and elongate, with the most common morphology being regular circular smaller burrows (75 to 450 μm diameter). A few irregular larger burrows (1800 μm diameter) are present. Burrow or tube coatings vary in orientation; however, they are frequently aligned parallel or oblique to adjacent burrows and form crude bedding parallel to the precipitating surface. Within non-burrow pores, lithoclastic and bioclastic grains of silt to fine sand (30 to 230 μm diameter) are common.

This facies has gradational contacts to facies 2, and crude bedding parallel to original tufa stromatolite laminae (Figs 8F and 9A). The gradational contact shows spar, micrite, organic matter and filamentous structures described in

© 2025 The Author(s). *Sedimentology* published by John Wiley & Sons Ltd on behalf of International Association of Sedimentologists,

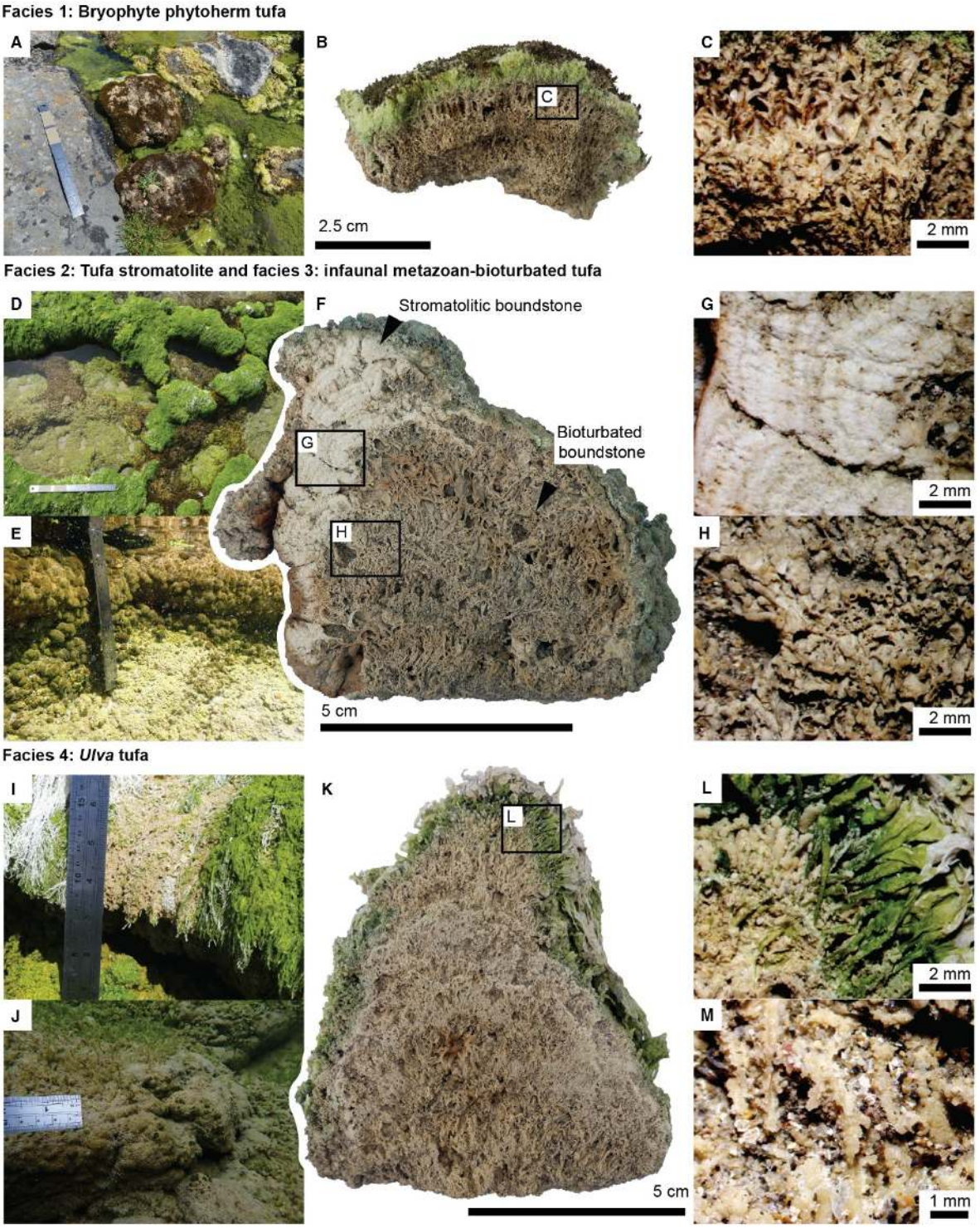


Fig. 8. Facies macrostructure. (A–C) Facies 1: bryophyte phytoherm tufa: (A) in-field photograph; (B) cross-section; (C) detail of internal structure showing bryophyte coatings. (D–H) Facies 2: tufa stromatolite and facies 3: infaunal metazoan-bioturbated tufa: (D) in-field photograph of barrage; (E) underwater photograph within barrage pool; (F) barrage cross-section of both stromatolitic and infaunal metazoan-bioturbated tufa; (G) detail of internal structure of tufa stromatolite; (h) detail of internal structure of infaunal metazoan-bioturbated tufa. (I–M) Facies 4: *Ulva* tufa: (I) in-field photograph of coated *Ulva* on barrage crest; (J) underwater photograph of uncoated *U. intestinalis* growing on tufa stromatolite; (K) barrage cross-section; (L) *U. intestinalis* on outer edge of barrage with basal carbonate coatings; (M) detail of internal structure. For in-field photographs, see 30 cm rule for scale.

© 2025 The Author(s). *Sedimentology* published by John Wiley & Sons Ltd on behalf of International Association of Sedimentologists, *Sedimentology*, **72**, 2173–2200

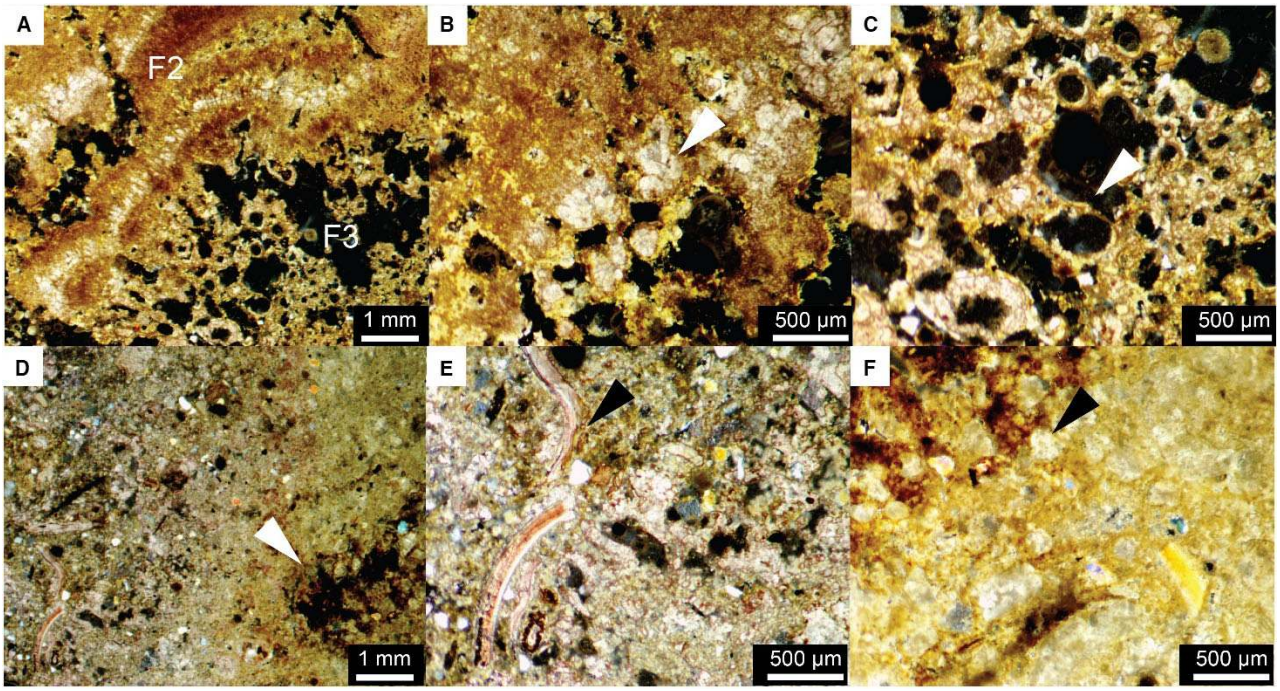


Fig. 9. Facies thin sections under XPL: (A–C) Facies 2: tufa stromatolite and facies 3: infaunal metazoan-bioturbated tufa (A) thin section showing gradational contact between upper tufa stromatolite (F2) and lower infaunal metazoan-bioturbated tufa facies (F3); (B) detail of disaggregated spar crystals within spar lamina (arrowed); (C) detail of burrow porosity within reworked spar, micrite, organic matter and microbial filaments (arrowed). (D–F) Facies 4: *Ulva* tufa: (D) thin section showing concentration of organic matter (*U. intestinalis* thallus) (arrowed); (E) detail of litho- and bio-clastic sand with mollusc shell clast (arrowed); (F) detail of spar crystals (arrowed) around organic matter (thallus).

facies 2, becoming increasingly disaggregated, forming abundant interparticle and burrow porosity (total porosity of 54.99%) (Fig. 9B, C).

Facies 4: Ulva tufa

Ulva tufa comprises boundstone of *U. intestinalis*, growing perpendicular to the precipitating surface but frequently lying prostrate when subaerially exposed in stacked parallel layers (ca 1 to 2 cm thick) forming crude bedding (Fig. 8K). Tubular thalli are coated in sparry calcium carbonate coatings from their base (Fig. 8L), and where thalli are not present, a moldic porosity is present, with variable porosity dependent on the degree of cementation (Fig. 8M). The moldic porosity of this facies is similar in morphology to metazoan burrows in cross-section; however, pores are compressed ovoid in section (Fig. 8M). Sand-size lithic inclusions and biological inclusions (e.g. fragments of *Mytilus edulis*, *Littorina littorea* shells and spines of *Paracentrotus lividus*) are common, including between uncemented *U. intestinalis* thalli. In thin section, a relatively homogenous and amorphous matrix of detrital and organic matter, micrite and spar intraclasts (ca 100 to 250 µm diameter) with low interparticle porosity (3.04%) is described (Fig. 9D, E), with concentrations of organic matter (ca 1 mm diameter), interpreted as *U. intestinalis* thalli (Fig. 9D), surrounded by spar crystals and the aforementioned detrital material (Fig. 9E, F).

Tufa facies distribution and associations

Bryophyte phytoherms (facies 1) are present at sites 1 to 3 and 5, typically in the upper supratidal zone above ca 5 m a.s.l. (site 3) extending into the terrestrial zone (backing cliffs). They occur on cascades and form the upper part of barrage crests, where they may be partially submerged and/or extend subaerially above water level. This facies occurs discretely as individual phytoherms (Fig. 8A) or on top of tufa stromatolite and infaunal metazoan-bioturbated tufa.

© 2025 The Author(s). *Sedimentology* published by John Wiley & Sons Ltd on behalf of International Association of Sedimentologists,

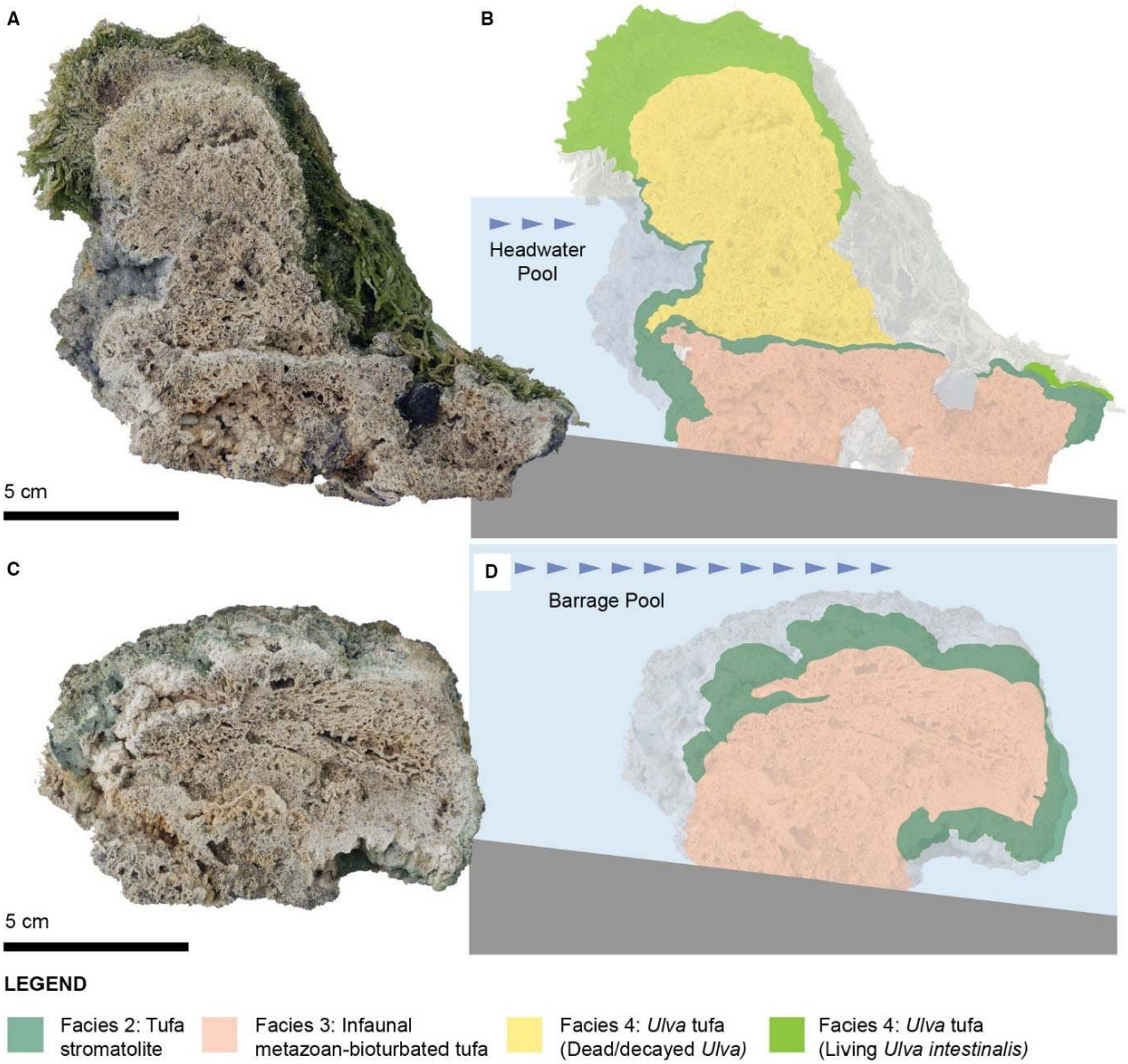


Fig. 10. Barrages composed of multiple facies. (A, B) Subaerial barrage impounding a headwater pool (site 3): (A) cross-section; (B) facies interpretation. (C, D) Submerged barrage (site 3): (A) cross-section; (B) facies interpretation.

Tufa stromatolite (facies 2) is present at all sites in the upper supratidal zone, above ca 3 m a.s.l. (site 3) and is typically subaqueous (Fig. 8E), although subaerial exposure is common at barrage pool and topographic basin perimeters. This facies occurs as cascades, barrages and fluvial and lacustrine crusts, although its greatest development is within barrage pools with barrages formed of facies 4 (Figs 8D and 9A, B). It may also form submerged barrages within barrage pools (Fig. 10A, B).

Infaunal metazoan-bioturbated tufa (facies 3) is present in sites 1 to 3, typically in the upper supratidal zone. It is primarily observed within barrages and cascades and is present beneath one or more laminae of tufa stromatolite (facies 2) (Fig. 10A to D) or exposed at eroded inactive deposits.

© 2025 The Author(s). *Sedimentology* published by John Wiley & Sons Ltd on behalf of International Association of Sedimentologists, *Sedimentology*, **72**, 2173–2200

Table 2. Barrage morphometric and physical parameter descriptive statistics of all measured barrages (n = 216) from all five study sites: site 1 (n = 38), site 2 (n = 26), site 3 (n = 84), site 4 (n = 3) and site 5 (n = 65).

	Mean ± 1SD	Median	Minimum–Maximum (Range)
Morphometric parameters			
Barrage crest width (m)	0.206 ± 0.145	0.159	0.062 to 1.102 (0.955)
Barrage straight length (m)	1.096 ± 1.035	0.842	0.229 to 8.543 (8.314)
Exposed drop wall height (m)	0.052 ± 0.056	0.037	−0.36 to 0.362 (0.398)
Total drop wall height (m)	0.084 ± 0.083	0.055	0.002 to 0.0676 (0.674)
Headwater pool distance (m)	0.775 ± 1.686	0.332	0.08 to 15.175 (15.095)
Tailwater pool distance (m)	0.0649 ± 1.233	0.346	0.077 to 12.525 (12.448)
Physical parameters			
Barrage crest elevation (m a.s.l.)	5.14 ± 2.395	4.114	1.945 to 9.379 (7.434)
Deposit dip (°)	5.14 ± 2.98	4.7	0.22 to 19.05 (18.83)
Inter-barrage dip (°)	7.29 ± 5.83	5.87	0 to 36.66 (36.66)

Ulva tufa (facies 4) is present at sites 1 to 3 and 5 in the lower supratidal zone below ca 4 to 4.7 m a.s.l. (site 3) and extending to the high tide mark. It occurs primarily as tall barrages, primarily subaerially (Fig. 8I) but may be partially submerged within barrage pools (Fig. 8J). The lowest elevation barrages are composed of only this facies. At its upper elevation limits, this facies is associated with facies 2 and 3, where *Ulva* tufa occurs as barrages, active/living *U. intestinalis* grows subaerially and dead/decayed *Ulva* occur within the barrage in association with subaqueous tufa stromatolite in the headwater pool (coating the *Ulva* tufa and lining the pool) and infaunal metazoan-bioturbated tufa at the base of barrages and barrage pool deposits (Fig. 10A, B).

Barrage morphometric and physical parameters

Measured barrage morphometric parameters are presented in Table 2. Barrages range in elevation from 1.945 to 9.379 m a.s.l., with inter-site variability linked to the available accommodation space on the shore platform profile.

Non-parametric correlation analysis

All barrage morphometric parameters are (0.01 significance level) positively correlated with one another (i.e. each barrage morphometry parameter increases as the others do) (Table 3). Most correlations are moderate (correlation coefficient 0.4 to 0.69), and the strongest correlations are between related parameters (e.g. barrage drop wall exposed height and total height: correlation coefficient: 0.815 at 0.01 sig.).

All barrage morphometric parameters increase with decreasing elevation AMSL at a 0.01 significance level; however, these correlations are weak (correlation coefficient: −0.25 to −0.34) or moderate (barrage crest width: correlation coefficient: −0.42) (Table 3). Correlation of slope and barrage morphometric parameters is variable dependent on the measure of slope (deposit dip or inter-barrage dip); however, the two measures themselves are only weakly correlated. Deposit dip is significantly positively correlated with barrage straight length and exposed drop wall height and negatively correlated with headwater and tailwater pool distances. Inter-barrage dip is statistically significantly correlated with barrage crest width, exposed drop wall height, total drop wall height and negatively correlated with tailwater pool distance (Table 3).

Observation and DSM visualisation of geomorphological response

Slope

The Pollraghly shore-platform has a shallow overall slope (3.83 to 8.71°) defined by bedrock

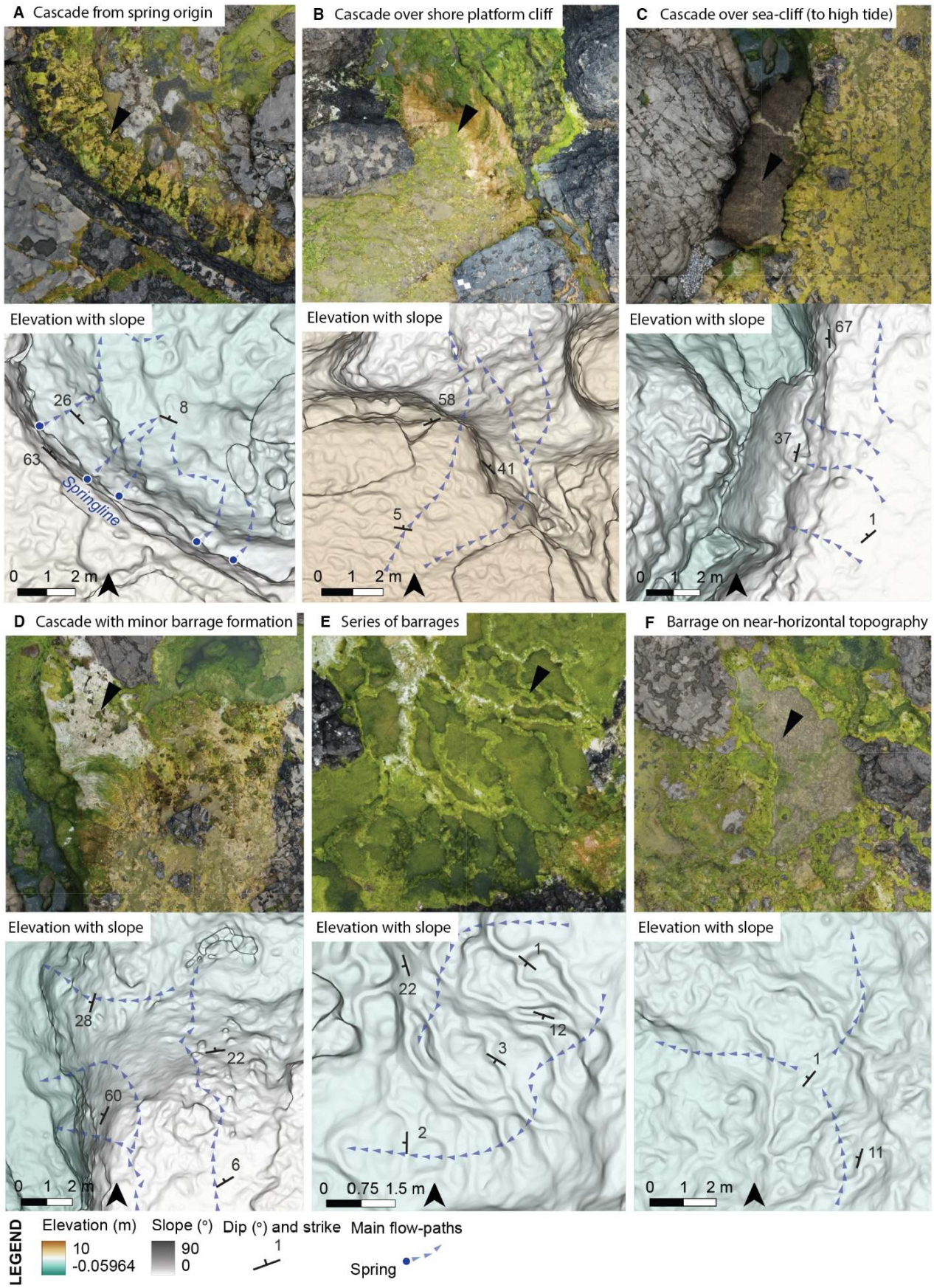
© 2025 The Author(s). *Sedimentology* published by John Wiley & Sons Ltd on behalf of International Association of Sedimentologists,

Table 3. Spearman's rank (rho) summary table; correlation coefficient, significance (two-tailed), number of observations (N).

			Barrage crest width (m; 3 s.f.)	Barrage straight length (m; 3 s.f.)	Barrage drop wall exposed height (m; 3 s.f.)	Barrage drop wall total height (m; 3 s.f.)	Headwater pool distance (m; 3 s.f.)	Tailwater pool distance (m; 3 s.f.)	Barrage crest elevation (m; 3 s.f.; AMSL)	Deposit dip (degrees; 2 s.f.;ThreePoint Method of deposit)	Inter-barrage dip (degrees; 2 s.f.;parameter-derived)
Spearman's rho	Barrage crest width (m; 3 s.f.)	Correlation Coefficient									
		Sig. (two-tailed)									
		N									
	Barrage straight length (m; 3 s.f.)	Correlation Coefficient	0.457**								
		Sig. (two-tailed)	<0.001								
		N	216								
	Barrage drop wall exposed height (m; 3 s.f.)	Correlation Coefficient	0.618**	0.393**							
		Sig. (two-tailed)	<0.001	<0.001							
		N	216	216							
	Barrage drop wall total height (m; 3 s.f.)	Correlation Coefficient	0.651**	0.555**	0.815**						
		Sig. (two-tailed)	<0.001	<0.001	<0.001						
		N	216	216	216						
	Headwater pool distance (m; 3 s.f.)	Correlation Coefficient	0.431**	0.600**	0.307**	0.420**					
		Sig. (two-tailed)	<0.001	<0.001	<0.001	<0.001					
		N	214	214	214	214					
	Tailwater pool distance (m; 3 s.f.)	Correlation Coefficient	0.402**	0.568**	0.457**	0.702**	0.423**				
		Sig. (two-tailed)	<0.001	<0.001	<0.001	<0.001	<0.001				
		N	216	216	216	216	214				
	Barrage crest elevation (m; 3 s.f.; AMSL)	Correlation Coefficient	−0.416**	−0.290**	−0.249**	−0.338**	−0.330**	−0.286**			
		Sig. (two-tailed)	<0.001	<0.001	<0.001	<0.001	<0.001	<0.001			
		N	216	216	216	216	214	216			
	Deposit dip (degrees; 2 s.f.; ThreePointMethod of deposit)	Correlation Coefficient	−0.113	−0.326**	0.158*	0.050	−0.340**	−0.235**	0.047		
		Sig. (two-tailed)	0.096	<0.001	0.021	0.464	<0.001	<0.001	0.496		
		N	216	216	216	216	214	216	216		
	Inter-barrage dip (degrees; 2 s.f.; parameter-derived)	Correlation Coefficient	0.251**	−0.100	0.532**	0.200**	−0.058	−0.415**	0.020	0.397**	
		Sig. (two-tailed)	<0.001	0.144	<0.001	0.003	0.396	<0.001	0.772	<0.001	
		N	216	216	216	216	214	216	216	216	

* Correlation is significant at the 0.05 level (two-tailed). ** Correlation is significant at the 0.01 level (two-tailed).

© 2025 The Author(s). *Sedimentology* published by John Wiley & Sons Ltd on behalf of International Association of Sedimentologists, *Sedimentology*, **72**, 2173–2200



© 2025 The Author(s). *Sedimentology* published by John Wiley & Sons Ltd on behalf of International Association of Sedimentologists, *Sedimentology*, **72**, 2173–2200

Fig. 11. Different geomorphological responses to variable slope of bedrock/underlying substrate. (A–C) Tufa cascades: (A) from spring line emergence (site 2); (B) over erosional cliff (site 5); (C) inactive cascade over erosional cliff with base at high tide (site 1). (D) Tufa cascade with minor barrage formation enhanced by potholing (site 1). (E, F) 'Typical' tufa barrages at variable slope: (E) a series of tufa barrages (site 1); (F) large tufa barrage on near-horizontal topography (site 2).

bedding; however, within study sites, a full range of bedrock slopes is observed, from sub-horizontal bedrock up to sub-vertical slopes at bedrock steps. Field observations and DSM visualisation show the steeper bedrock slope is associated with the cascade morphology, while the shallower bedrock slope is associated with barrages, lacustrine and fluvial crusts. Cascades are present at bedding steps (ca 90°) and larger scale erosional surfaces of multiple beds (cliff-faces dipping at ca 20 to 90°) that occur across the shore platform profile: from spring emergence (Fig. 11A); mid-platform over bedding steps and cliffs (Fig. 11B); and at seaward cliffs that frequently plunge to the high tide line (Fig. 11C). Rarely, the cascade morphology impounds water, producing small barrage structures (Fig. 11D). Tufa barrages occur in areas of medium slope (bedrock dipping at ca 0 to 20°) across the shore platform. Barrages on steeper slopes (up to ca 20°; Fig. 11E) are smaller, with smaller barrage pool distances; and barrages on shallow slopes (ca 1°; Fig. 11F) are larger, with large barrage pools. Lacustrine crusts occur in topographic bedrock basins and fluvial crusts occur across the full range of slopes (ca 0 to 90°).

Bedrock topography

After groundwater spring emergence, water flows seaward across the shore platform ranges from unconstrained flow forming discharge aprons and delta-like arrangements of barrages to fully constrained flow in discrete channels. The degree of constraint/channelisation and channel width varies along flow paths as water drains across the shore platform and influences barrage morphology. At site 1, for example, large barrages are developed within a broad channel in the headwaters that can extend as single or few large barrages across the channel. The flowpath changes at a downstream cliffline, where it exits the channelised section, and flow is no longer constrained, producing a large delta-like system of barrages (Fig. 12A).

Straight and parallel barrages are associated with bedrock steps (Fig. 12B) Bedrock topographic highs above the surrounding barrage pool water level can also be connected by barrages (Fig. 12C). 'Compound' barrages (barrage pools occurring within larger barrages) occur within large, thick barrages, especially those with large exposed dropwalls (Fig. 12C). Submerged subaqueous barrages are also present in the largest barrage pools where they form complex bifurcating patterns (Fig. 12B).

Elevation

The Pollraghly shore-platform is topographically complex; however, site 3 has a consistent supratidal slope of ca 4 to 6°, defined by bedrock bedding, with minor bedrock steps (Fig. 5E). This provides insight into the variability in geomorphology with respect to elevation AMSL, controlled for slope. Scatterplots (Fig. 13A) demonstrate variation in barrage morphometric parameters across the flow pathway.

Barrage crest width does not vary considerably across the elevation profile; however, barrage straight length is greatest around 3.5 to 4.25 m AMSL. Barrage total and exposed drop wall height is also greatest at this elevation; however, in this zone, barrage total exposed drop wall height is considerably greater than average height, both on the upper bedding plane and below the bedding step. Barrage pool length (headwater and tailwater) also conforms to this pattern (Fig. 13A). The upper occurrence of *U. intestinalis* between ca 4.7 and 0 m a.s.l. coincides with this zone of barrages composed of multiple facies including Ulva tufa (facies 4) with larger pools and greater drop wall height (Fig. 13C). Smaller barrage pools composed of tufa stromatolite (facies 2) occur above (ca > 4.7 m a.s.l.) (Fig. 13B).

DISCUSSION

Occurrence and distribution

The uniformity of groundwater spring temperature, pH and EC (Table 1) demonstrates a shared karstic groundwater aquifer origin within calcarenite limestone bedrock, of meteogene

© 2025 The Author(s). *Sedimentology* published by John Wiley & Sons Ltd on behalf of International Association of Sedimentologists, *Sedimentology*, **72**, 2173–2200

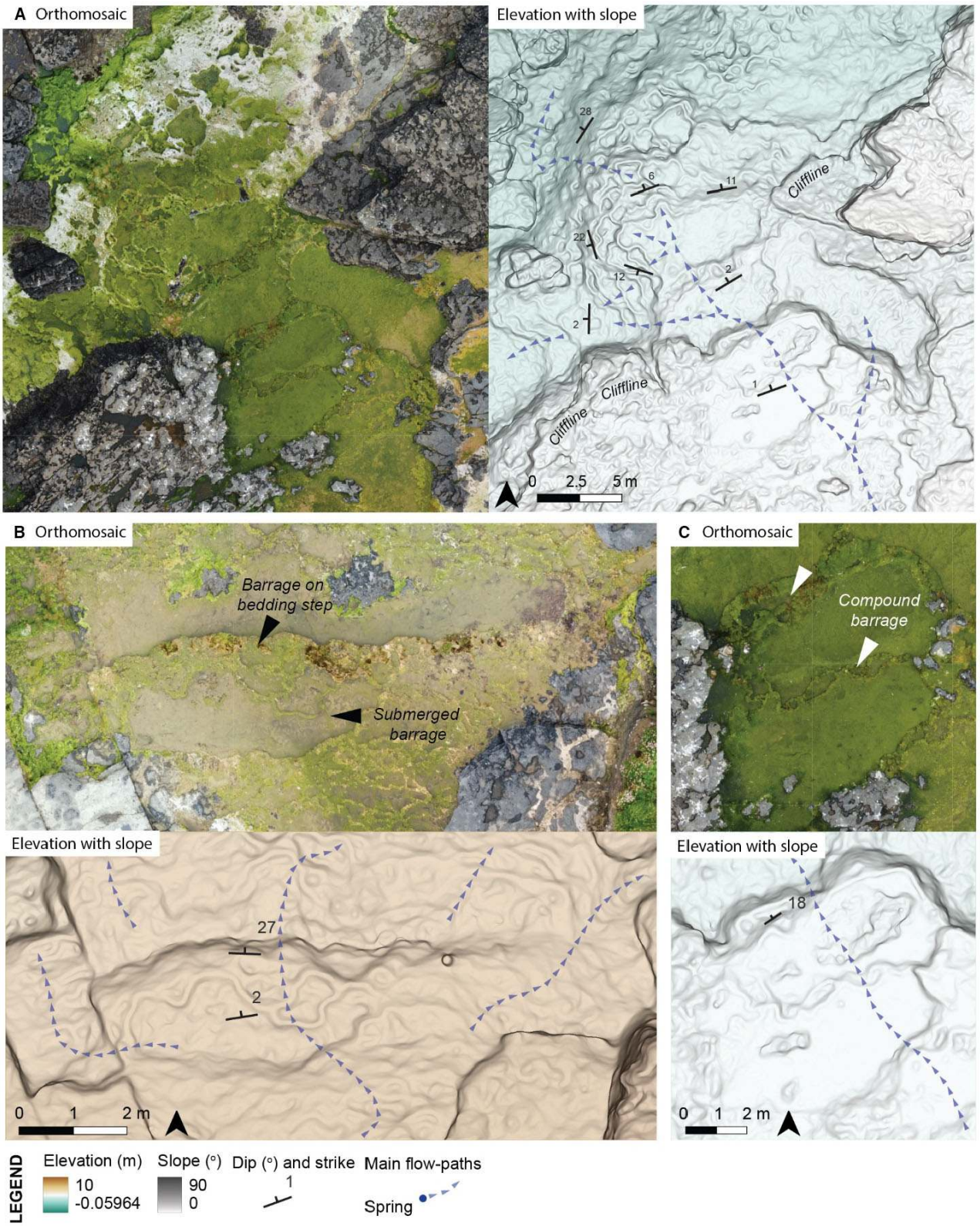


Fig. 12. (A) Transition from channelised tufa barrages to 'delta'-like feature (site 1). (B) Barrage formation on topographic break in bedding (bedding step) (site 5). (C) 'Compound' barrage formation with barrage pool formation within large barrage between bedrock outcrops (site 1).

© 2025 The Author(s). *Sedimentology* published by John Wiley & Sons Ltd on behalf of International Association of Sedimentologists, *Sedimentology*, **72**, 2173–2200

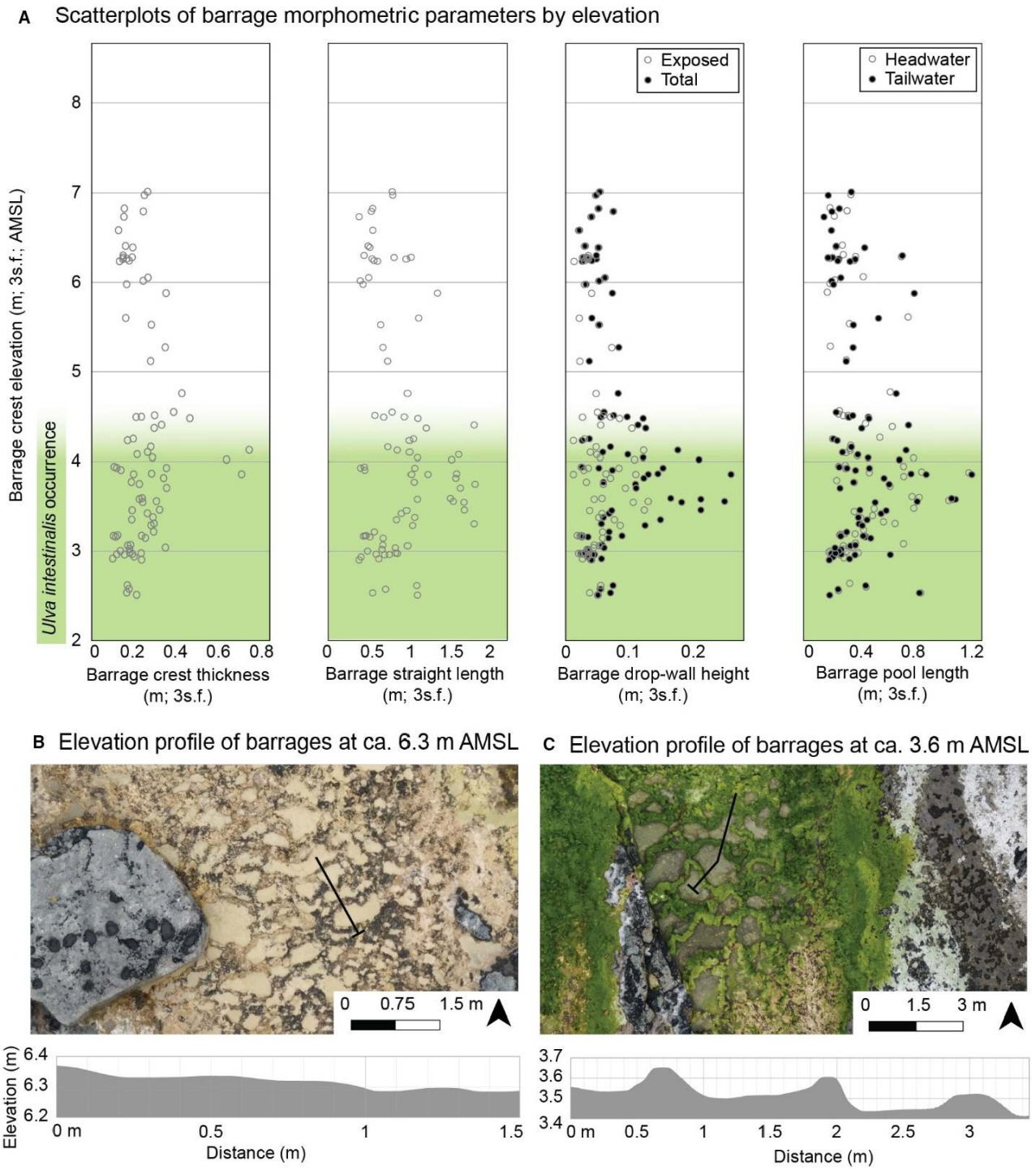


Fig. 13. Variation in barrage morphology with elevation. (A) Scatterplots of barrage morphometric parameters by elevation AMSL, with *U. intestinalis* occurrence (0 to 4.75 m a.s.l.) in green. (B, C) Elevation profile (cross-sections) of barrages with orthomosaic showing cross-section position (black line): (B) tufa stromatolite barrages at ca 6.3 m a.s.l.; (C) multi-facies barrages including *Ulva* tufa at ca 3.6 m a.s.l.

© 2025 The Author(s). *Sedimentology* published by John Wiley & Sons Ltd on behalf of International Association of Sedimentologists, *Sedimentology*, **72**, 2173–2200

groundwater likely of calcium-bicarbonate type expected of the Beltra–Sligo groundwater body (GSI, 2004).

Due to the supratidal distribution of deposits, barrage pools exhibit variable physico-chemistry, attributable to spatial (e.g. proximity to marine input and elevation) and temporal (e.g. seasonal variability in storminess) variables. Barrage pool temperature varies, attributed to seasonal air temperature with pool-specific variability due to pool depth and morphology, exposure and elevation. The circum-neutral to alkaline pH is variable, comparable to other supratidal tufa localities [Western Australian: 7 to 9.5 and South African: 7.3 to 9.2 (Forbes *et al.*, 2010, 2024; Dodd *et al.*, 2018)], due to the amount of photosynthetic activity and saltwater mixing within barrage pools. Variability in EC is associated with variation in elevation AMSL, topography (e.g. degree of protection by outcropping bedrock, dip and aspect) and seasonal high-water events. The degree of mixing with marine-derived saltwater through sea spray/splash and wave overtopping results in seasonal haloclines as demonstrated by the high EC (Rishworth *et al.*, 2017b; Dodd *et al.*, 2018).

Following spring emergence, carbonate deposition on the shore platform occurs from 9.5 m a.s.l. (site 5) and ceases at the high tide limit (1.625 m); firmly locating these deposits within the supratidal (supralittoral or splash) zone. The distribution of coastal tufa occurrences in the tidal frame is poorly quantified. Regionally, microbial mats and tufa deposits have described as supratidal and high intertidal at the Giant's Causeway, Northern Ireland (Cooper *et al.*, 2013), supratidal in Cornwall, England (Howie & Ealey, 2009, 2011; Howie *et al.*, 2012) and from the supratidal zone 'near to sea-level' at Lismore, Scotland (Faulkner & Crae, 2018, 2022). South African rock coast microbialites exhibit their greatest development in the supratidal zone and 'stunted' development in the intertidal zone (Smith *et al.*, 2011, 2018; Perissinotto *et al.*, 2014; Edwards *et al.*, 2017; Rishworth *et al.*, 2017b, 2020; Dodd *et al.*, 2018, 2021; du Plooy *et al.*, 2020); however, no quantified elevation data is given. Australian tufa occurrences are described from the intertidal and supratidal zone (Forbes *et al.*, 2010).

Tufa facies formation and zonation

The four tufa facies forming large-scale supratidal tufa barrages in the study involve distinct biological mediators ('bio-mediated tufa' of Ford & Pedley (1996)) with cross-shore zonation. The facies association described demonstrates a clear seaward facies zonation from bryophyte phytoherm tufa (>6 m a.s.l.) to tufa stromatolite and infaunal metazoan-bioturbated tufa (<3 m a.s.l.) to *Ulva* tufa (<4 to ca 1.6 m a.s.l.) at high tide. This facies zonation is derived from the ecological zonation of the facies formative biological mediator. Due to intersecting elevation ranges, multi-facies complex barrages occur (Fig. 14A). Zonation elevations are derived from Site 3: Pollcam has a consistent supratidal slope of ca 4 to 6°, hence, slope and other environmental variables (e.g. water velocity) do not need to be accounted for when establishing a zonation.

Bryophyte tufa (or phytoherm framestone) is a common facies of spring carbonate deposits (Pedley, 1990; Pentecost & Viles, 1994; Pentecost, 2005; Jones & Renaut, 2010; Lyons & Kelly, 2021), with plants acting as a substrate for calcium carbonate precipitation. Following encrustation, the internal decay of bryophytes produces highly porous tufa with distinctive structure, based on the growth pattern and structure of the formative plants (Pentecost, 2005; Jones & Renaut, 2010). Their occurrence in the high supratidal zone likely marks the limit of purely terrestrial conditions.

The distribution of this facies is likely constrained by salinity tolerance, as tufa-associated bryophytes in Ireland are absent, incidental or non-persistent from supratidal coastal settings if subjected to saline spray/splash (Hill *et al.*, 2007; Lyons & Kelly, 2021). Local hydrological conditions also influence its distribution as bryophyte phytoherms tend to be subaerial, present on cascades and on the top of barrages. Bryophytes remain moist through splashing and capillary action, resulting in basal calcium carbonate encrustation and progressive increase in barrage height (Pentecost, 2005).

Tufa stromatolite (or phytoherm boundstone or stromatolitic tufa) is a known facies of terrestrial (Pedley, 1990; Jones & Renaut, 2010) and supratidal (Perissinotto *et al.*, 2014; Edwards *et al.*, 2017; Smith *et al.*, 2018; Rishworth *et al.*, 2020; Forbes *et al.*, 2024) spring carbonate deposits. Its development is attributed to microorganisms and associated biofilms that mediate tufa stromatolite growth through the surface precipitation of calcium carbonate, with some trapping and binding (Riding, 1991; Jones & Renaut, 2010). The colloform mesostructure (Garner *et al.*, 2024) displays concentric

© 2025 The Author(s). *Sedimentology* published by John Wiley & Sons Ltd on behalf of International Association of Sedimentologists,

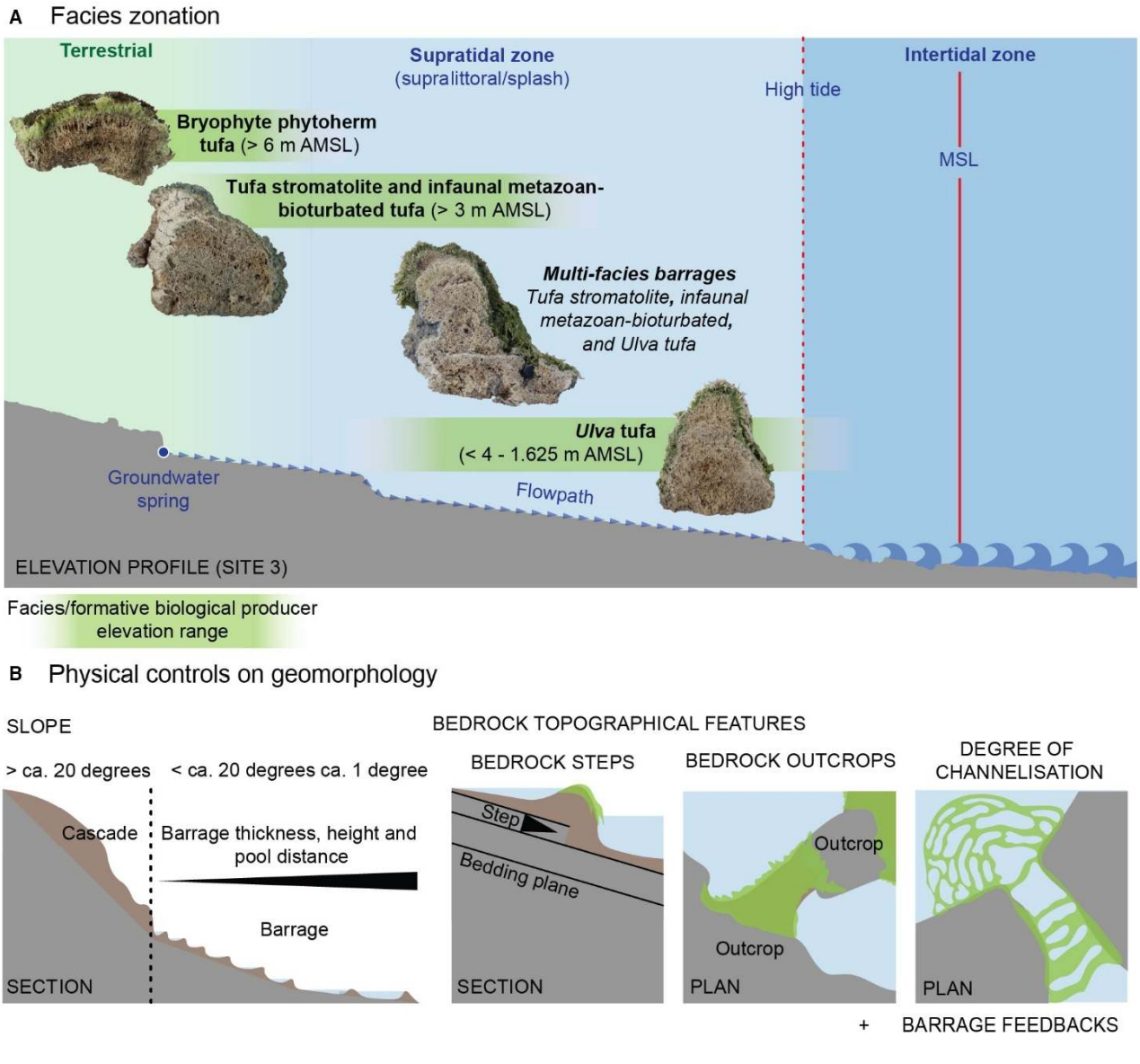


Fig. 14. Summary of (A) facies zonation and (B) physical controls on geomorphology.

lamination in section with clusters of filamentous cyanobacteria normal to lamination, and as such can be considered biologically mediated and laminated (i.e. stromatolitic). Other rock coast tufa barrages are dominated by tufa microbialites, including phytoherm framestone with *Vaucheria*-like algal filaments in Western Australia (Forbes *et al.*, 2010) and tufa microbialite in South Africa (Edwards *et al.*, 2017).

The controls and drivers of this facies in the supratidal zone include a complex suite of factors including geology, pool physico-chemistry and hydrology, primary producers and ecology (e.g. grazers, bioturbators, consumers); described in detail by Rishworth *et al.* (2020). Regarding elevation, the distribution of tufa stromatolites is likely to be constrained by substrate and groundwater spring physico-chemistry, notably salinity tolerance (Dodd *et al.*, 2018).

The infaunal metazoan-bioturbated tufa facies is a modified tufa stromatolite in which the original laminated fabric is disrupted (e.g. by tube-forming) or destroyed by the activities of metazoan communities (Edwards *et al.*, 2017; Rishworth *et al.*, 2019; Dodd *et al.*, 2021). Evidence for reworking comes from crude bedding

© 2025 The Author(s). *Sedimentology* published by John Wiley & Sons Ltd on behalf of International Association of Sedimentologists, *Sedimentology*, **72**, 2173–2200

and clear gradational contact with the tufa stromatolite facies. This reworked fabric has been attributed to infaunal metazoan communities (oligiochaetes, amphipods, tanaidids and polychaetes) in South African and Western Australian supratidal tufa deposits (Weston *et al.*, 2018; Rishworth *et al.*, 2019; Dodd *et al.*, 2021) and is attributed to oligochaetes, amphipods, chironomid larvae, ostracods, nematodes and dasyhelean larvae in Pollraghly shore platform tufa deposits (Rishworth, pers. comm.). The increase in porosity from 5.41 to 54.99%, and the occurrence of lithic grains within pores is comparable to the passive (opposed to trapping and binding) sediment accumulation reported from South African metazoan-bioturbated tufa or 'rimstone' deposits with porosities of 44.95 to 67.63% (Edwards *et al.*, 2017; Dodd *et al.*, 2021). Infaunal metazoans also produce distinctive larval constructions that undergo cementation to produce distinct facies in terrestrial carbonates (Carthew *et al.*, 2002; Ben Ahmed *et al.*, 2018); however, the absence of external larval constructions on the exterior of barrages and the clear gradational contact between tufa stromatolite and bioturbated tufa facies (Fig. 9A) supports a bioturbation origin (Edwards *et al.*, 2017; Rishworth *et al.*, 2019; Dodd *et al.*, 2021). However, further research should be undertaken to understand the timing of precipitation in relation to infaunal metazoan constructions. The distribution of infaunal metazoan-bioturbated tufa is intrinsically associated with the tufa stromatolite facies through its reworked nature.

Ulva intestinalis acts as a substrate for carbonate precipitation with subsequent decay producing a porous boundstone with a distinctive structure or bio-fabric. The biological mediation of calcium carbonate precipitation appears to be comparable to the formation of extracellular crystals of calcium carbonate on thalli of *Ulva flexuosa* subsp. *pilifera* (Messyasz *et al.*, 2013), and calcium carbonate (aragonite) within the closed tubular thallus and thallus base in *Blidingia minima (*formerly *Enteromorpha nana*) (Dodson, 1974). The degree of facilitation of calcium carbonate precipitation is unclear; however, thalli clearly act as a surface for spar precipitation. Sand-sized lithic and biological inclusions within carbonate-coated and uncoated surficial thalli suggest that the sand inclusions are actively baffled by the *U. intestinalis* thalli. Green macro-algae have the potential to outcompete and degrade tufa microbialite crusts (Doddy *et al.*, 2019; Rishworth *et al.*, 2020). The absence of metazoan burrows or tube-forming may reflect the exclusion of infaunal metazoan grazers or bioturbators via periodic emergence (Budd & Pizzola, 2008) in this primarily subaerial facies. While *Ulva* and green macro-algae are associated with infaunal metazoan-bioturbated tufa in the intertidal margin in South Africa (Rishworth *et al.*, 2020) and with 'tidal barrages' on the Isle of Lismore (Faulkner & Crae, 2018), *Ulva* tufa has not previously been identified as a supratidal rock coast spring carbonate facies.

The elevation occurrence and distribution of *Ulva* tufa (facies 4) appears determined by the ecological constraints of *U. intestinalis*. *U. intestinalis* is common on coasts of Britain and Ireland, abundant in brackish water with appreciable freshwater run-off and wet areas of the splash zone (Budd & Pizzola, 2008); hence, supratidal groundwater springs thus offer an ideal habitat. Rodríguez Guitián *et al.* (2020) describe *Ulva*-associated tufa deposition where wave action is moderate but not strong.

The relationship between barrage geomorphology and facies is obscured by the presence of individual barrages composed of multiple facies (e.g. *Ulva* tufa barrage with tufa microbialite). Elevation is significantly (0.01 sig.) negatively correlated with all barrage morphometric parameters, indicating that larger barrages form at lower elevations. The occurrence of *U. intestinalis* between ca 4.7 and 0 m a.s.l. coincides with larger barrages (Fig. 13), suggesting *Ulva* tufa forms barrages with tall, exposed barrage dropwalls, aided by its tolerance to desiccation and subaerial emersion. *U. intestinalis* survives desiccation as the uppermost layers bleach because moisture is retained beneath the bleached thalli (Budd & Pizzola, 2008). This ability to survive subaerially and high recoverability to smothering and rapid reproduction/colonisation (Budd & Pizzola, 2008) may allow continued fast growth and recolonisation during/after encrustation of the thalli base with calcium carbonate. Similarly, the ability for bryophyte phytoherm tufa to develop through basal calcium carbonate encrustation through capillary action (Pentecost, 2005) allows for bryophyte phytoherms to produce larger subaerial deposits (exposed drop wall height). While thin tufa stromatolite crusts are observed subaerially around bedrock basin and barrage pool rims, they are primarily subaqueous and are limited to these pools. Thus, they are restricted to subaqueous environments and consequently unable to form substantial subaerial barrage crests comparable to bryophyte phytoherm tufa and *Ulva* tufa.

© 2025 The Author(s). *Sedimentology* published by John Wiley & Sons Ltd on behalf of International Association of Sedimentologists,

Globally, other barrage-forming rock coast tufa occurrences are dominated by tufa microbialites of autochthonous phytoherm framestone (Edwards *et al.*, 2017; Rishworth *et al.*, 2020; Garner *et al.*, 2024). While comparable facies (tufa stromatolite and infaunal metazoan-bioturbated tufa) are present on the Pollraghly shore platform, the adjacent bryophyte phytoherm tufa and *Ulva* tufa facies remain poorly known elsewhere. While *Ulva* and green macro-algae are associated with rimstone mesofabric (infaunal metazoan-bioturbated tufa) in the intertidal margin (Rishworth *et al.*, 2020) and with 'tidal' barrages (Faulkner & Crae, 2018), their role in calcium carbonate precipitation is unclear. Green macro-algae have the potential to outcompete and degrade tufa microbialite crusts (Doddy *et al.*, 2019; Rishworth *et al.*, 2020). At Pollraghly, the zonation AMSL indicates that exposure to fully marine conditions (i.e. littoral and sublittoral) is a primary control of macroalgae occurrence, but further investigation of its role in tufa precipitation is sought.

Physical controls on barrage geomorphology

The facies association is primarily determined by elevation AMSL; however, physical controls contribute added complexity to barrage geomorphology (Fig. 14B).

Slope

DSM visualisation and non-parametric correlation analysis demonstrates the control of slope on barrage morphology, notably barrage pool distance. Cascades form on bedrock dipping at ca 20 to 90°, and barrages form when bedrock dips at ca 1 to 20°; within this range, steeper slopes are associated with smaller pool distances. This matches the relationship established in other tufa barrage settings (Pentecost, 2005; Hammer *et al.*, 2007; Vázquez-Urbez *et al.*, 2012; Florsheim *et al.*, 2013). Following initial deposition, flow dynamics are modified, promoting further tufa deposition and growth of tufa deposits in a positive feedback, decreasing slope and accommodation space (Chan & Goldenfeld, 2007; Hammer *et al.*, 2007; Florsheim *et al.*, 2013).

Bedrock topography

Tufa geomorphology responds to variable degrees of channelisation and constraint as water drains over the rock platform. Channel width and degree of channelisation/constraint are established as a control on barrage development and geomorphology due to their influence on flow hydrodynamics (Pedley, 1980, 1990; Fuller *et al.*, 2011; Florsheim *et al.*, 2013; Profe *et al.*, 2016). Channel constrictions can initiate barrage formation by increasing flow velocity and promoting channel-spanning barrages (Pedley, 1980, 1990; Fuller *et al.*, 2011). Channel expansions have also been proposed to promote tufa deposition due to a greater air–water interface (Merz-Preiß & Riding, 1999; Chen *et al.*, 2004; Florsheim *et al.*, 2013). A full range of channel constraints akin to those found in fluvial barrage systems exists on the Pollraghly shore platform, and while channel constraint has a major influence on barrage geomorphology, barrages are not strictly limited to either constrictions or channel widening.

Bedrock topographical features such as steps in longitudinal profile (bedrock steps) and prominent outcrops both influence barrage initiation and development on the shore platform. Topographical features such as bedrock steps (Fuller *et al.*, 2011; Banks *et al.*, 2012), erosion resistant bedrock (Kempe & Emeis, 1985; Pedley, 1990; Carthew *et al.*, 2003) and local obstructions or slope breaks (Lambert, 1955; Pentecost & Viles, 1994; Hammer *et al.*, 2008; Vázquez-Urbez *et al.*, 2012; Florsheim *et al.*, 2013), all have been described as initiating, or are associated with, barrages. The initiation substrate can control barrage plan morphology. Just as fallen trees produce regular planform barrages in streams (Carthew *et al.*, 2003), bedrock steps initiate straight, parallel barrages. In this sense, barrages initiated by bedrock steps function as small cascades in response to bedrock topography that impound water, further suggesting a shared genesis and continuum between these two morphologies. The potential for topographic steps to influence barrage development downstream of topographic steps (Profe *et al.*, 2016) is also demonstrated at Pollraghly, where tufa is absent in the extreme upper shore platform at sites 1 and 5, suggesting the threshold for calcium carbonate precipitation is not met due to hydrodynamic, topographical (i.e. little variation in topography) and biological (i.e. lack of biomediators) factors, initiated downstream.

The gently sloping (ca 9 to 3.5°) Pollraghly shore platform defined by shallow seaward-dipping bedrock of uniform lithology, with some bedrock steps and erosional surfaces, contrasts with tufa occurrences on South African rock coasts. Steeply dipping bedrock of variable

© 2025 The Author(s). *Sedimentology* published by John Wiley & Sons Ltd on behalf of International Association of Sedimentologists, *Sedimentology*, **72**, 2173–2200

bedrock lithology forms discontinuous ridges and gullies, resulting in barrage and pool formation being structurally controlled by irregular bedrock topography (Edwards *et al.*, 2017).

Compound barrages occur on thick primary barrages, potentially forming through the modification of the primary barrage (Carthew *et al.*, 2003). Submerged, or 'drowned' (Pedley, 1990), barrages have been suggested elsewhere to be the result of a headwater pool submerging an upstream barrage due to downstream barrage development, in a competitive process where precipitation and barrage growth rate are integral (Hammer *et al.*, 2007; Hammer, 2009). Submersion reduces precipitation through the weakening of precipitation via positive feedback (Hammer, 2009). The concept of competitive barrage development in producing submerged barrages, however, does not sufficiently explain their occurrence in supratidal barrages because the submerged barrages are composed of subaqueous tufa stromatolite and infaunal metazoan-bioturbated tufa facies. If submerged barrages were a consequence of competitive barrage development, then *Ulva* tufa would be observed beneath the tufa stromatolite/infaunal metazoan-bioturbated tufa facies: a facies association that is not present in submerged barrages (Fig. 10A, B).

Comparison of morphometry and controls on tufa geomorphology

Comparing barrage morphometry of Pollraghly shore platform barrages to global occurrences demonstrates that these deposits are all similar in their scale and likely controls. However, Pollraghly shore platform barrages exhibit an average width of 20 cm (±13.5 cm), ranging from 6 cm to 1.1 m, compared to South African localities that exhibit far wider barrages (up to 1 m). The extensive width of the latter is due to persistent pool haloclines (Dodd *et al.*, 2018), preventing basal accretion and forming wide overhangs (Edwards *et al.*, 2017). Examination of the physico-chemical conditions and potential occurrence of haloclines in barrage pools at Pollraghly shore platform may offer insight into the absence of substantial overhangs and differences in global morphology.

Total dropwall height ranges from 0.002 to 0.676 m with a mean of 0.084 ± 0.083 m, comparable to global occurrences; however, the mean is notably smaller than barrage heights of <0.1 to 0.3 m reported in Western Australia (Forbes *et al.*, 2010) and up to 1 m deep in South Africa (Edwards *et al.*, 2017). This may be partly attributable to difficulty in assessing total depth through UAV photogrammetry but more likely results from differing bedrock topography. Headwater and tailwater pool distances are repeated parameters from different barrage measurements and, as such, have near identical values and distributions (Table 2). The mean pool distance is 0.775 ± 1.686 m, comparable to the lower estimates of barrage pools in Western Australia (<1 m to 5 m) (Forbes *et al.*, 2010) and South Africa (<1 m to 7 m diameter) (Edwards *et al.*, 2017); however, there is a considerably large range (up to 15.175 m pool distance). Evident in global localities, there is potential for the under-recognition of smaller barrage features, with an emphasis on the largest enigmatic features that may not be representative of wider barrage morphologies.

Bryophyte-dominated fluvial barrage tufa with riparian vegetation (Viles & Pentecost, 1999; Pentecost *et al.*, 2001) is primarily channelised with barrages spanning the channel, and channel width acting as a primary control on barrage straight length. For example, Pentecost *et al.* (2001) reported 1 to 10 m-wide barrages that fully span the channel. While channel-spanning barrages are present in the study area (e.g. site 1), the complex topography on the shore platform creates high variability in channel width. Other fluvial morphometric parameters are similar, including pool distance and heights, the latter of 0.03 to 1.32 m (mean 0.25 m) (Viles & Pentecost, 1999) and 0.02 to 0.46 m (mean 0.29 m) (Pentecost *et al.*, 2001) are similar to the Pollraghly shore platform barrage heights of 0.002 to 0.676 m (mean 0.084 ± 0.083 m). However, at Pollraghly, smaller barrages up to 0.002 m high, less than GSD resolution, occur suggesting a continuum exists extending to close to 0 cm, as observed in the field.

Fundamentally, the rock coast shore platform environment differs from terrestrial tufa occurrences as rock coasts are typically hostile as sedimentary environments (Trenhaile, 2016). The conceptual framework for interactions between biological-geomorphological processes in travertine s.l., development proposed by Fuller *et al.* (2011) identifies biological and ecological dynamics that are absent or weak in the shore platform setting. For example, colonisation by carbonate-encrusting plants such as bryophytes (e.g. *Eucladium verticllatum*) and coastal

© 2025 The Author(s). *Sedimentology* published by John Wiley & Sons Ltd on behalf of International Association of Sedimentologists,

specialist vascular plants (e.g. *Armeria maritima*) is limited to the upper supratidal and terrestrial zones. In addition, 'trapping of floating organic material', is limited to floating masses of *U. intestinalis* in barrage pools.

The key differences between shore platform and 'terrestrial' barrage tufa deposits are:

- The degree and type of biological mediation.
- The substantial reduction/absence of emergent vegetation.
- The absence of substantial riparian vegetation, including fallen trees, complex root systems, leaf accumulations and LWD.
- Direct exposure to storms and extreme wave events (Cooper *et al.*, 2004; O'Brien *et al.*, 2018).
- Impacts of saline waters via inundation, splash and spray.

Extreme wave events have been noted to cause substantial damage to supratidal rock coast tufa microbialites in South Africa (Smith *et al.*, 2020; Garner, 2024); however, the long-term effects of destructive events on the net geomorphological balance are poorly understood. The occurrence of substantial megaclastic coastal boulder deposits (Cox *et al.*, 2017; Cox, 2020) on the west coast of Ireland indicates the regular occurrence of high-magnitude wave events that traverse the shore platform.

In terrestrial settings, the positive feedback wherein precipitation modifies bed morphology to favour tufa precipitation (Chen *et al.*, 2004; Hammer *et al.*, 2008; Chin *et al.*, 2014; Zhang *et al.*, 2023) is counteracted by destructive events (e.g. high discharge, flooding and debris flow events (Fuller *et al.*, 2011)) resulting in negative feedback, ultimately producing a long-term steady-state condition. A balancing act that considers the biological, physical and chemical extrinsic forces for microbialite accretion is modelled by Reid *et al.* (2024) may extend to tufa microbialites and other bio-mediated tufa deposits, including those described here.

CONCLUSION

The first quantified elevation distributions for tufa occurrences in the rock coast environment firmly place deposits within the supratidal zone and limit them by the high tide mark. However, deposits do experience saltwater inundation within the splash zone. Tufa facies are formed by various biological mediators that lead to comparable facies to other global occurrences, including tufa stromatolite and infaunal metazoan-bioturbated (rimstone) tufa. The novel *Ulva* tufa facies has not previously been reported in the rock coast setting despite the occurrence of *Ulva* at other global localities.

The distribution of these tufa facies reflects the ecological zonation of their biological mediators, from terrestrial bryophyte phytoherm tufa (>6 m a.s.l.) to tufa stromatolite and infaunal metazoan-bioturbated tufa (<3 m a.s.l.) to *Ulva* tufa (<4 to ca 1.6 m a.s.l.) and precipitation ceases at the high tide mark. Where the distribution of these biological mediators intersects, multi-facies complex barrages occur that can offer insight into the formation of barrages due to the environmental and ecological preferences of their formative biological producers (e.g. facies associations suggest submerged barrage formation cannot be simply explained by 'drowning' by downstream barrages). Facies directly control the macro-structure or macro-morphology of barrages.

The abiotic control on tufa geomorphology is demonstrated through DSM and orthomosaic visualisation and non-parametric correlation analysis. Slope is a dominant control on barrage geomorphology, fitting with the established pattern of smaller barrage pools on steeper slopes. Bedrock topography is highly variable in the rock coast shore platform environment and as a result, a variety of topographies result in a diverse assemblage of barrage geomorphologies, influenced by variable degrees of channelisation, channel width, bedrock steps and erosional surfaces. There are clear differences between South African occurrences and the Pollraghly shore platform occurrences in bedrock topography (derived from structural geological and lithological differences), facies and morphometry. There are also significant differences in the biological controls between supratidal rock coast tufa and their terrestrial counterparts, in particular the absence of emergent plants and riparian vegetation. The identification of supratidal deposition and facies elevation limits suggests that tufa deposits can be utilised as Quaternary palaeo-sea-level archives on rock coasts in emergent settings.

ACKNOWLEDGEMENTS

This research was made possible through the NERC-funded EPStromNet project (NERC reference NE/V00834X/1) and a Department for the Economy (DfE) sponsorship for postgraduate

© 2025 The Author(s). *Sedimentology* published by John Wiley & Sons Ltd on behalf of International Association of Sedimentologists, *Sedimentology*, **72**, 2173–2200

studentship. The authors thank David Rogers for UAV operation and photogrammetry processing; supervisor Joerg Arnscheidt for assistance with in-field water physico-chemistry measurement and the EPStromNet team for in-field discussion and support.

DATA AVAILABILITY STATEMENT

UAV derived datasets are available from the corresponding author upon reasonable request; derived measurements are provided as supplementary information. All other data used in the publication are completely and directly provided in the manuscript.

REFERENCES

Andrews, J.E. (2006) Palaeoclimatic records from stable isotopes in riverine tufas: synthesis and review. *Earth Sci. Rev.*, **75**, 85–104.

Arp, G., **Wedemeyer, N.** and **Reitner, J.** (2001) Fluvival tufa formation in a hard-water creek (Deinschwanger Bach, Franconian Alb, Germany). *Facies*, **44**, 1–22.

Banks, V.J., **Jones, P.F.**, **Lowe, D.J.**, **Lee, J.R.**, **Rushton, J.** and **Ellis, M.A.** (2012) Review of tufa deposition and palaeohydrological conditions in the White Peak, Derbyshire, UK: implications for Quaternary landscape evolution. *Proc. Geol. Assoc.*, **123**, 117–129.

Ben Ahmed, W., **Henchiri, M.**, **Mastouri, A.** and **Slim S'himi, N.** (2018) Calcified aquatic insect larval constructions in the Pleistocene tufa of Jebel El Mida, Gafsa, southern Tunisia: recognition and paleoenvironmental significance. *J. African Earth Sci.*, **140**, 256–266.

Brach, E. (2023) ThreePointMethod Plugin for QGIS (Plugin ID:2875). Version 1.0. https://github.com/ThreePointPlugin/ThreePoint. Accessed 20 February 2025.

Budd, G.C. and **Pizzola, P.F.** (2008) *Ulva intestinalis Gut weed. Marine Life Information Network: Biology and Sensitivity Key Information Reviews*. Marine Biological Association of the United Kingdom, Plymouth.

Capezzuoli, E., **Gandin, A.** and **Pedley, M.** (2014) Decoding tufa and travertine (fresh water carbonates) in the sedimentary record: the state of the art. *Sedimentology*, **61**, 1–21.

Carter, C.D. and **Marks, J.C.** (2007) Influences of travertine dam formation on leaf litter decomposition and algal accrual. *Hydrobiologia*, **575**, 329–341.

Carthew, K.D., **Taylor, M.P.** and **Drysdale, R.N.** (2002) Aquatic insect larval constructions in tropical freshwater limestone deposits (TUFA): preservation of depositional environments. *Gen. Appl. Entomol. J. Entomol. Soc. N. S. W.*, **31**, 35–41.

Carthew, K.D., **Taylor, M.** and **Drysdale, R.** (2003) Are current models of tufa sedimentary environments applicable to tropical systems? A case study from the Gregory River. *Sediment. Geol.*, **162**, 199–218.

Chan, P.Y. and **Goldenfeld, N.** (2007) Steady states and linear stability analysis of precipitation pattern formation at geothermal hot springs. *Phys. Rev. E*, **76**, 046104.

Chen, J., **Zhang, D.D.**, **Wang, S.**, **Xiao, T.** and **Huang, R.** (2004) Factors controlling tufa deposition in natural waters at waterfall sites. *Sediment. Geol.*, **166**, 353–366.

Chin, A., **Florsheim, J.L.**, **Wohl, E.** and **Collins, B.D.** (2014) Feedbacks in Human–Landscape Systems. *Environ. Manag.*, **53**, 28–41.

Compson, Z.G., **Mier, M.Z.** and **Marks, J.C.** (2009) Effects of travertine and flow on leaf retention in Fossil Creek, Arizona. *Hydrobiologia*, **630**, 187–197.

Cooper, J.A.G., **Jackson, D.W.T.**, **Navas, F.**, **McKenna, J.** and **Malvarez, G.** (2004) Identifying storm impacts on an embayed, high-energy coastline: examples from western Ireland. *Mar. Geol.*, **210**, 261–280.

Cooper, A., **Smith, A.** and **Arnscheidt, J.** (2013) Contemporary stromatolite formation in high intertidal rock pools, Giant's Causeway, Northern Ireland: preliminary observations. *J. Coast. Res.*, **165**, 1675–1680.

Cooper, A., **Smith, A.**, **Rishworth, G.**, **Dodd, C.**, **Forbes, M.**, **Cawthra, H.** and **Anderson, C.** (2022) Microbialites of modern siliciclastic rock coasts. *J. Sediment. Res.*, **92**, 619–634.

Cox, R. (2020) Megagravel deposits on the west coast of Ireland show the impacts of severe storms. *Weather*, **75**, 72–77.

Cox, R., **Jahn, K.**, **Watkins, O.** and **Cox, P.** (2017) Extraordinary boulder transport by storm waves (West of Ireland, Winter 2013–2014), and criteria for analysing coastal boulder deposits. *Earth Sci. Rev.*, **20**, 14.

Della Porta, G. (2015) Carbonate build-ups in lacustrine, hydrothermal and fluvial settings: comparing depositional geometry, fabric types and geochemical signature. In: *Microbial Carbonates in Space and Time: Implications for Global Exploration and Production* (Eds Bosence, D.W.J., Gibbons, K.A., Heron, D.P.L., Morgan, W.A., Pritchard, T. and Vining, B.A.), *Geological Society of London*, **418**, 487–495.

Dodd, C., **Anderson, C.R.**, **Perissinotto, R.**, **du Plooy, S.J.** and **Rishworth, G.M.** (2018) Hydrochemistry of peritidal stromatolite pools and associated freshwater inlets along the Eastern Cape coast, South Africa. *Sediment. Geol.*, **373**, 163–179.

Dodd, C., **Anderson, C.R.**, **Rishworth, G.M.**, **Perissinotto, R.** and **van Niekerk, X.** (2021) Metazoan activity facilitates passive sediment trapping in modern supratidal microbialites: revealed using μ-CT-scanning and microscopy. *Geobiology*, **19**, 585–600.

Doddy, P., **Roden, C.M.** and **Gammell, M.P.** (2019) Nutrient pollution degrades microbialites in Lough Carra, an Irish marl lake. *Aquat. Microb. Ecol.*, **83**, 203–209.

Dodson, J. (1974) Calcium carbonate formation by *Enteromorpha nana* algae in a hypersaline volcanic crater lake. *Hydrobiologia*, **44**, 247–255.

Drysdale, R. and **Gillieson, D.** (1997) Micro-erosion meter measurements of travertine deposition rates: a case study from Louie Creek, Northwest Queensland, Australia. *Earth Surf. Process. Landf.*, **22**, 1037–1051.

Edwards, M.J.K., **Anderson, C.R.**, **Perissinotto, R.** and **Rishworth, G.M.** (2017) Macro- and meso-fabric structures of peritidal tufa stromatolites along the Eastern Cape coast of South Africa. *Sediment. Geol.*, **359**, 62–75.

Faulkner, T. and **Crae, J.** (2018) Distribution of tufa and speleothem deposits on the Island of Lismore, Argyll, Scotland. *Cave Karst. Sci.*, **45**, 101–110.

Faulkner, T. and **Crae, J.** (2022) Exotic tufa and speleothem deposits on the calcareous Island of Lismore, Argyll,

Scotland. In: *Published in the Proceedings of the 18th International Congress of Speleology*. Savoie-Technolac, France, pp. 55–58.

Flinn, D. and **Pentecost, A.** (1995) Travertine-cemented screes on the serpentinite seacliffs of Unst and Fetlar, Shetland. *Mineral Mag.*, **59**, 259–265.

Florsheim, J.L., **Ustin, S.L.**, **Tang, Y.**, **Di, B.**, **Huang, C.**, **Qiao, X.**, **Peng, H.**, **Zhang, M.** and **Cai, Y.** (2013) Basin-scale and travertine dam-scale controls on fluvial travertine, Jiuzhaigou, southwestern China. *Geomorphology*, **180–181**, 267–280.

Forbes, M., **Vogwill, R.** and **Onton, K.** (2010) A characterisation of the coastal tufa deposits of south–west Western Australia. *Sediment. Geol.*, **232**, 52–65.

Forbes, M., **Rishworth, G.**, **Underwood, G.**, **Cooper, A.**, **Garner, T.**, **Hicks, N.**, **Dodd, C.**, **Mcgenity, T.**, **Smith, A.**, **Cawthra, H.**, **Adams, J.** and **Clark, D.** (2024) *Rocky Coastline Bio-Mediated Carbonate Deposits: Quaternary Archive, Modern Environmental Stress Indicator or Both?* Australian Quaternary Association, North Stradbroke Island.

Ford, T.D. and **Pedley, H.M.** (1996) A review of tufa and travertine deposits of the world. *Earth Sci. Rev.*, **41**, 117–175.

Fuller, B., **Sklar, L.**, **Compson, Z.**, **Adams, K.**, **Marks, J.** and **Wilcox, A.** (2011) Ecogeomorphic feedbacks in regrowth of travertine step-pool morphology after dam decommissioning, Fossil Creek, Arizona. *Geomorphology*, **126**, 314–332.

Garner, T. (2024) Awards: quaternary microbialite facies of Eastern Cape of South Africa. *Quat. Res. Assoc. Quat. Newsl.*, **162**, 40–43.

Garner, T., **Cooper, J.A.G.**, **Smith, A.M.**, **Rishworth, G.** and **Forbes, M.** (2024) Reviews and syntheses: tufa microbialites on rocky coasts – towards an integrated terminology. *Biogeosciences*, **21**, 4785–4807.

Garner, T.W., **Cooper, J.A.G.** and **Smith, A.** (2025) Marginal marine spring carbonates defining an emergent rocky shoreline at Cape Freycinet, Western Australia. *Mar. Geol.*, **481**, 107496.

Google Earth Pro. (2025) Google Earth Pro. https://earth.google.com/web/. Accessed 20 February 2025.

GSI. (2004) Beltra-Sligo GWB: summary of initial characterisation. https://gsi.geodata.gov.ie/downloads/Groundwater/Reports/GWB/BeltraSligoGWB.pdf. Accessed 20 February 2025.

GSI. (2019) Quaternary Sediments 1:50,000 Ireland (ROI) ITM. https://data.gov.ie/dataset/quaternary-sediments-150000-ireland-roi-itm. Accessed 20 February 2025.

GSI. (2021) Bedrock Geology 1:100,000 Ireland (ROI) ITM. https://data.gov.ie/dataset/bedrock-geology-1100000-ireland-roi-itm. Accessed 20 February 2025.

Hägele, D., **Leinfelder, R.**, **Grau, J.**, **Burmeister, E.-G.** and **Struck, U.** (2006) Oncoids from the river Alz (southern Germany): tiny ecosystems in a phosphorus-limited environment. *Palaeogeogr. Palaeoclimatol. Palaeoecol.*, **237**, 378–395.

Hammer, Ø. (2009) Pattern formation by local amplification and lateral inhibition: examples from biology and geology. *Eur. Phys. J. Spec. Top.*, **178**, 5–12.

Hammer, Ø., **Dysthe, D.K.** and **Jamtveit, B.** (2007) The dynamics of travertine dams. *Earth Planet. Sci. Lett.*, **256**, 258–263.

Hammer, Ø., **Dysthe, D.K.**, **Lelu, B.**, **Lund, H.**, **Meakin, P.** and **Jamtveit, B.** (2008) Calcite precipitation instability under laminar, open-channel flow. *Geochim. Cosmochim. Acta*, **72**, 5009–5021.

He, J., **Lin, J.** and **Xu, Y.** (2021) Modeling the Relationships between the Height and Spectrum of Submerged Tufa Barrage Using UAV-Derived Geometric Bathymetry and Digital Orthoimages. *Sensors*, **21**, 6987.

Herman, J.S. and **Lorah, M.M.** (1988) Calcite precipitation rates in the field: measurement and prediction for a travertine-depositing stream. *Geochim. Cosmochim. Acta*, **52**, 2347–2355.

Hill, M.O., **Preston, C.D.**, **Bosanquet, S.D.S.** and **Roy, D.B.** (2007) *BRYOATT - Attributes of British and Irish Mosses, Liverworts and Hornworts*. Centre for Ecology and Hydrology, Huntingdon.

Howie, F. and **Ealey, P.** (2009) Tufa and speleothem occurrence in north and west cornwall. *Geosci. South-West Engl.*, **12**, 109–114.

Howie, F. and **Ealey, P.** (2010) An appraisal of Quaternary calcium carbonate deposits in Cornwall. *Geosci. South-West Engl.*, **12**, 233–240.

Howie, F. and **Ealey, P.** (2011) Coastal tufa and speleothems of Prussia and Stackhouse coves, South-West Cornwall. *Geosci. South-West Engl.*, **12**, 278–288.

Howie, F., **Ealey, P.** and **Anderson, A.** (2012) Tufa, tufa-cemented rockfalls and speleothems of Newtrain Bay, North Cornwall. *Geosci. South-West Engl.*, **13**, 93–111.

Jackson, D.W.T., **Short, A.D.**, **Loureiro, C.** and **Cooper, J.A.G.** (2022) Beach morphodynamic classification using high-resolution nearshore bathymetry and process-based wave modelling. *Estuar. Coast. Shelf Sci.*, **268**, 107812.

Jones, B. and **Renaut, R.W.** (2010) Calcareous spring deposits in continental settings. In: *Developments in Sedimentology* (Eds Alonso-Zarza, A.M. and Tanner, L.H.), pp. 177–224. Elsevier, London.

Kempe, S. and **Emeis, K.** (1985) Carbonate chemistry and the formation of Plitvice Lakes. *Mitt. Geol-Paläontol. Inst. Univ. Hambg.*, **25**, 351–383.

Lambert, A. (1955) Remarques sur les depots de travertins par les cours d'eau et sur leurs consequences morphologiques [with discussion]. *Bull. Soc. Géol. Fr.*, **S6-V**, 577–588.

Lorah, M.M. and **Herman, J.S.** (1988) The chemical evolution of a travertine-depositing stream: geochemical processes and mass transfer reactions. *Water Resour. Res.*, **24**, 1541–1552.

Lu, G., **Zheng, C.**, **Donahoe, R.J.** and **Berry Lyons, W.** (2000) Controlling processes in a $CaCO_3$ precipitating stream in Huanglong Natural Scenic District, Sichuan, China. *J. Hydrol.*, **230**, 34–54.

Lyons, M.D. and **Kelly, D.L.** (2021) Rapid tufa deposition and bryophyte growth rates in Irish petrifying springs. *J. Bryol.*, **43**, 162–174.

Marine Institute. (2017) Collated Seabed Substrate. https://data.gov.ie/dataset/collated-seabed-substrate. Accessed 20 February 2025.

Merz-Preiß, M. and **Riding, R.** (1999) Cyanobacterial tufa calcification in two freshwater streams: ambient environment, chemical thresholds and biological processes. *Sediment. Geol.*, **126**, 103–124.

Messyasz, B., **Czerwik-Marcinkowska, J.**, **Massalski, A.**, **Uher, B.**, **Rybak, A.**, **Szendzina, L.** and **Pikosz, M.** (2013) Morphological and ultrastructural studies on *Ulva flexuosa* subsp. *pilifera* (Chlorophyta) from Poland. *Acta. Soc. Bot. Pol.*, **82**, 157–163.

Met Éireann. (2024) Ireland's 30-year Climate Averages. https://www.met.ie/climate/30-year-averages. Accessed 20 February 2025.

© 2025 The Author(s). *Sedimentology* published by John Wiley & Sons Ltd on behalf of International Association of Sedimentologists, *Sedimentology*, **72**, 2173–2200

O'Brien, L., **Renzi, E.**, **Dudley, J.M.**, **Clancy, C.** and **Dias, F.** (2018) Catalogue of extreme wave events in Ireland: revised and updated for 14 680 BP to 2017. *Nat. Hazards. Earth. Syst. Sci.*, **18**, 729–758.

Pedley, H.M. (1980) The occurrence and sedimentology of a Pleistocene travertine in the Fiddien Valley, Malta. *Proc. Geol. Assoc.*, **91**, 195–202.

Pedley, H.M. (1987) The Flandrian (Quaternary) Caerwys Tufa, North Wales: an ancient barrage tufa deposit. *Proc. Yorks Geol. Soc.*, **46**, 141–152.

Pedley, H.M. (1990) Classification and environmental models of cool freshwater tufas. *Sediment. Geol.*, **68**, 143–154.

Pentecost, A. (2005) *Travertine*. Springer, Berlin.

Pentecost, A. and **Viles, H.** (1994) A Review and Reassessment of Travertine Classification. *Géogr. Phys. Quat.*, **48**, 305–314.

Pentecost, A., **Peterken, G.** and **Viles, H.A.** (2001) The travertine dams of Slade Brook, Gloucestershire: their formation and conservation. *Geol. Today*, **16**, 22–25.

Perissinotto, R., **Bornman, T.G.**, **Steyn, P.-P.**, **Miranda, N.A.F.**, **Dorrington, R.A.**, **Matcher, G.F.**, **Strydom, N.** and **Peer, N.** (2014) Tufa stromatolite ecosystems on the South African south coast. *South Afr. J. Sci.*, **110**, 1–8.

du Plooy, S.J., **Rishworth, G.M.**, **Perissinotto, R.** and **Dodd, C.** (2020) Nutrient uptake and primary production in lithifying peritidal tufa stromatolites. *J. Exp. Mar. Biol. Ecol.*, **525**, 151314.

Profe, J., **Höfle, B.**, **Hämmerle, M.**, **Steinbacher, F.**, **Yang, M.-S.**, **Schröder-Ritzrau, A.** and **Frank, N.** (2016) Characterizing tufa barrages in relation to channel bed morphology in a small karstic river by airborne LiDAR topo-bathymetry. *Proc. Geol. Assoc.*, **127**, 664–675.

Reid, R.P., **Suosaari, E.P.**, **Oehlert, A.M.**, **Pollier, C.G.L.** and **Dupraz, C.** (2024) Microbialite accretion and growth: lessons from Shark Bay and the Bahamas. *Ann. Rev. Mar. Sci.*, **16**, 487–511.

Riding, R. (1991) *Calcareous Algae and Stromatolites*. Springer, Berlin.

Rishworth, G.M., **Perissinotto, R.**, **Bird, M.S.** and **Pelletier, N.** (2017a) Grazer responses to variable macroalgal resource conditions facilitate habitat structuring. *R. Soc. Open Sci.*, **5**, 171428.

Rishworth, G.M., **Perissinotto, R.**, **Bornman, T.G.** and **Lemley, D.A.** (2017b) Peritidal stromatolites at the convergence of groundwater seepage and marine incursion: patterns of salinity, temperature and nutrient variability. *J. Mar. Syst.*, **167**, 68–77.

Rishworth, G.M., **Edwards, M.J.K.**, **Cónsole-Gonella, C.** and **Perissinotto, R.** (2019) Modern active microbialite-metazoan relationships in peritidal systems on the Eastern Cape coast of South Africa: ecological significance and implication for the palaeontological record. *J. African Earth Sci.*, **153**, 1–8.

Rishworth, G.M., **Dodd, C.**, **Perissinotto, R.**, **Bornman, T.G.**, **Adams, J.B.**, **Anderson, C.R.**, **Cawthra, H.C.**, **Dorrington, R.A.**, **du Toit, H.**, **Edworthy, C.**, **Gibb, R.-L.A.**, **Human, L.R.D.**, **Isemonger, E.W.**, **Lemley, D.A.**, **Miranda, N.A.F.**, **Peer, N.**, **Raw, J.L.**, **Smith, A.M.**, **Steyn, P.-P.**, **Strydom, N.A.**, **Teske, P.R.** and **Welman, S.** (2020) Modern supratidal microbialites fed by groundwater: functional drivers, value and trajectories. *Earth Sci. Rev.*, **210**, 103364.

Rodríguez Guitián, M.A., **Real, C.**, **Ramil-Rego, P.**, **Franco, R.R.** and **Castro, H.L.** (2020) Characteristics, vulnerability and conservation value of active tufa-forming springs on coastal cliffs in the NW Iberian Peninsula. *Ocean Coast. Manag.*, **189**, 105122.

RPS Group. (2020) Mean Sea Level to OD Malin (OSGM15) Corrective Surface (ICWWS 2018 – Phase 4). https://data.gov.ie/dataset/mean-sea-level-to-od-malin-osgm15-corrective-surface-icwws-2018-phase-4. Accessed 20 February 2025.

Smith, A.M., **Andrews, J.E.**, **Uken, R.**, **Thackeray, Z.**, **Perissinotto, R.**, **Leuci, R.** and **Marca-Bell, A.** (2011) Rock pool tufa stromatolites on a modern South African wave-cut platform: partial analogues for Archaean stromatolites? *Terra Nova*, **23**, 375–381.

Smith, A., **Cooper, A.**, **Misra, S.**, **Bharuth, V.**, **Guastella, L.** and **Botes, R.** (2018) The extant shore platform stromatolite (SPS) facies association: a glimpse into the Archean? *Biogeosciences*, **15**, 2189–2203.

Smith, A., **Cooper, A.**, **Guastella, L.** and **Bharath, V.** (2020) Wave influences in contemporary and Mesoarchaean stromatolites. *Sediment. Geol.*, **396**, 105558.

Sunamura, T. (1992) *Geomorphology of Rocky Coasts*. Wiley, New York, NY.

Trenhaile, A. (2016) Rocky coasts — their role as depositional environments. *Earth Sci. Rev.*, **159**, 1–13.

Vázquez-Urbez, M., **Arenas, C.** and **Pardo, G.** (2012) A sedimentary facies model for stepped, fluvial tufa systems in the Iberian Range (Spain): the Quaternary Piedra and Mesa valleys. *Sedimentology*, **59**, 502–526.

Viles, H.A. and **Pentecost, A.** (1999) Geomorphological controls on tufa deposition at Nash Brook, South Wales. *Cave Karst. Sci.*, **26**, 589.

Weston, R.-L.A., **Perissinotto, R.**, **Rishworth, G.M.** and **Steyn, P.-P.** (2018) Macroinvertebrate variability between microhabitats of peritidal stromatolites along the South African coast. *Mar. Ecol. Prog. Ser.*, **605**, 37–47.

Wolfgang, D. and **Gabrovsek, F.** (2009) Small-scale Terraces and Isolated Rimstone Pools on Stalagmites in Caves Exhibit Striking Similarity to Large-scale Terrace Landscapes at Hot Springs. *Acta Carsologica.*, **38**, 19–26.

Zhang, T., **Dai, Q.**, **An, D.**, **Mors, R.A.**, **Li, Q.**, **Astini, R.A.**, **He, J.**, **Cui, J.**, **Jiang, R.**, **Dong, F.** and **Dang, Z.** (2023) Effective mechanisms in the formation of pool-rimstone dams in continental carbonate systems: the case study of Huanglong, China. *Sediment. Geol.*, **455**, 106486.

Manuscript received 1 April 2025; revision accepted 6 August 2025

© 2025 The Author(s). *Sedimentology* published by John Wiley & Sons Ltd on behalf of International Association of Sedimentologists, *Sedimentology*, **72**, 2173–2200